Old Dominion University

ODU Digital Commons

2022

Variability and Dynamics of Along-Shore Exchange on the West Antarctic Peninsula (WAP) Continental Shelf

Xin Wang

Carlos Moffat

Michael S. Dinniman
Old Dominion University, mdinnima@odu.edu

John M. Klinck
Old Dominion University, jklinck@odu.edu

David A. Sutherland

See next page for additional authors

Authors

Xin Wang, Carlos Moffat, Michael S. Dinniman, John M. Klinck, David A. Sutherland, and Borja Aguiar-Gonzáles

Variability and Dynamics of Along-Shore Exchange on the West Antarctic Peninsula (WAP) Continental Shelf

Xin Wang[1] , Carlos Moffat[1] , Michael S. Dinniman[2] , John M. Klinck[2] , David A. Sutherland[3] , and Borja Aguiar-González[1,4]

[1]College of Earth, Ocean and Environment, University of Delaware, Newark, DE, USA, [2]Center for Coastal Physical Oceanography, Old Dominion University, Norfolk, VA, USA, [3]Department of Earth Sciences, University of Oregon, Eugene, OR, USA, [4]Departamento de Física, Universidad de Las Palmas de Gran Canaria, Las Palmas de Gran Canaria, Spain

Abstract The continental shelf of the West Antarctic Peninsula (WAP) is characterized by strong along-shore hydrographic gradients resulting from the distinct influences of the warm Bellingshausen Sea to the south and the cold Weddell Sea water flooding Bransfield Strait to the north. These gradients modulate the spatial structure of glacier retreat and are correlated with other physical and biochemical variability along the shelf, but their structure and dynamics remain poorly understood. Here, the magnitude, spatial structure, seasonal-to-interannual variability, and driving mechanisms of along-shore exchange are investigated using the output of a high-resolution numerical model and with hydrographic data collected in Palmer Deep. The analyses reveal a pronounced seasonal cycle of along-shore transport, with a net flux (7.0×10^5 m³/s) of cold water toward the central WAP (cWAP) in winter, which reverses in summer with a net flow (5.2×10^5 m³/s) of Circumpolar Deep Water (CDW) and modified CDW (mCDW) toward Bransfield Strait. Significant interannual variability is found as the pathway of a coastal current transporting Weddell-sourced water along the WAP shelf is modulated by wind forcing. When the Southern Annual Mode (SAM) is positive during winter, stronger upwelling-favorable winds dominate in Bransfield Strait, leading to offshore advection of the Weddell-sourced water. Negative SAM leads to weaker upwelling- or downwelling-favorable winds and enhanced flooding of the cWAP with cold water from Bransfield Strait. This process can result in significant (0.5°C below 200 m) cooling of the continental shelf around Palmer Station, highlighting that along-shore exchange is critical in modulating the hydrographic properties along the WAP.

Plain Language Summary The melting of glaciers and the structure of ecosystems along the West Antarctic Peninsula have been influenced by the local temperature and salinity patterns. Our understanding of what controls the spatial structure and temporal variability of these gradients is limited. In this study, we analyze output from a state-of-the-art numerical model and find that there is strongly seasonal and interannual variability in the along-shore exchange processes that control those gradients. The interannual variability of the along-shore exchange is related to the local winds. As the wind conditions vary in response to hemispheric-scale climate processes, the amount of cold water flowing into the central West Antarctic Peninsula from Bransfield Strait varies interannually. We show this is a key process in the evolution of ocean properties in the West Antarctic Peninsula continental shelf.

1. Introduction

Observations dating back to the 1950s show that the West Antarctic Peninsula (WAP) has undergone remarkable long-term atmospheric warming in the Southern Hemisphere prior to the 2000s (Turner et al., 2005; Vaughan et al., 2003), with the warming trends weakening or reversing since then (Clem et al., 2019; Oliva et al., 2017; Turner et al., 2016). This and other changes in atmospheric and open ocean forcing conditions have led to widespread changes in the physical environment and ecosystem structure in the WAP, including ocean warming (Schmidtko et al., 2014), glacier retreat (Cook et al., 2005, 2016), duration of the sea-ice season (Stammerjohn et al., 2008), and changes in marine productivity (Montes-Hugo et al., 2009). One of the key features of the oceanic structure in this region is a strong along-shore gradient in hydrographic properties, which is characterized by relatively warm deep waters in the southern part of the WAP shelf, and cold waters in Bransfield Strait (Figure 1). This gradient has been suggested to directly modulate or at least correlate with major observational trends in this region. Glacier retreat rates along the WAP are higher in the southern central WAP (cWAP) dominated by the warmer subsurface waters (Cook et al., 2016). This pattern is also evident in observed changes in phytoplankton
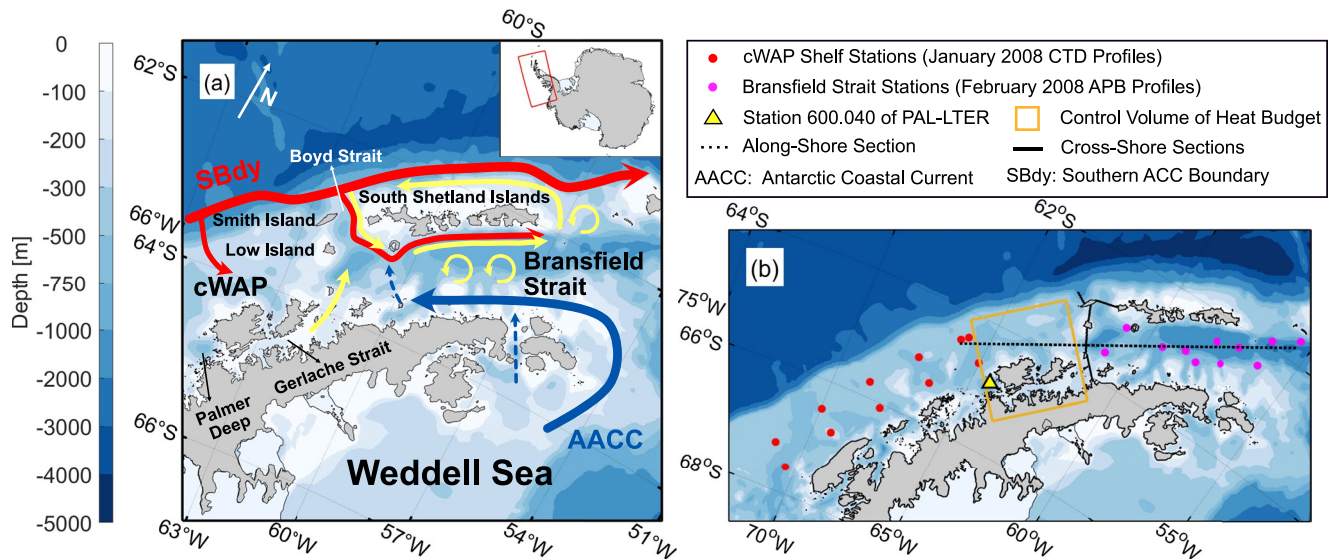
Figure 1. (a) Overview of the circulation on the West Antarctic Peninsula (WAP) shelf based on previous studies (e.g., Dotto et al., 2016; Moffat & Meredith, 2018; Niiler et al., 1991; Sangrà et al., 2011, 2017; Savidge & Amft, 2009; Thompson et al., 2009; Zhou et al., 2002, 2006). Inset shows the model domain. (b) Locations of hydrographic measurements were used in this study on the central WAP shelf (red) and in Bransfield Strait (magenta). The dotted line shows the location of the along-shore section in Figure 4. The solid lines indicate the location of the cross-shore sections and Boyd Strait section in Figure 6 and Figure 8. The orange box shows the region used for the heat budget calculations in Figure 14. The yellow triangle shows the location of station 600.040 of the Palmer Long Term Ecological Research sampling grid. Blue shading in both panels is the bathymetry.

distribution. From 1978 to 1986 to 1998–2006, chlorophyll concentrations decreased significantly in the northern region (roughly north of Anvers Island) while decreasing to the south, highlighting a strong pattern of along-shore variability (Montes-Hugo et al., 2009).

The feature that forms the boundary between the cWAP and Bransfield Strait, and that we will call the Southern Bransfield Front (SBF), is formed by the distinct bathymetry and hydrographic processes on either side of the front. To the south, the upper water column in the cWAP is dominated by Antarctic Surface Water (AASW), which is characterized by large seasonal variations due to air-sea buoyancy fluxes, sea-ice formation and melting, and wind-induced mixing (Hofmann et al., 1996; D. A. Smith et al., 1999). Winter Water (WW) is formed from deep cooling of the surface layer during the winter and is characterized by a temperature minimum below the AASW during summer. Below WW, a modified version of the oceanic Circumpolar Deep Water (CDW) dominates the deep layer of the shelf, acting as a source of heat, salt, and some macronutrients. Modified CDW (mCDW, <1.5°C, 34.50 to 34.72) is formed by cooling and freshening of CDW as a result of vertical heat and salt loss to the surface layers, and the melting of glaciers and ice shelves (D. A. Smith & Klinck, 2002; Moffat et al., 2009; Moffat & Meredith, 2018). Mesoscale eddies are critical for the delivery of CDW to the cWAP and this water mass is preferentially carried onshore in the large submarine troughs typical of the bathymetry of this region (Couto et al., 2017; Martinson & McKee, 2012; Moffat et al., 2009). Near the coast, a main feature of the circulation is the Antarctic Coastal Current (AACC, in prior work, the Antarctic Peninsula Coastal Current–APCC), a narrow, coastally-trapped current flowing along the WAP (Moffat et al., 2008; Savidge & Amft, 2009; Schubert et al., 2021). The mCDW-dominated deep layer and the upper layers, with WW and AASW, form the southern boundary of the SBF.

Bransfield Strait occupies the northeast of the WAP, forming a semi-enclosed basin located between the main coast of the Antarctic Peninsula and the South Shetland Islands that connects to the north-western Weddell Sea (Figure 1). The first order current structure in Bransfield Strait is a cyclonic gyre with a southwestward branch, a cold and strongly barotropic form of the AACC (or CC in previous work), which carries water from the Weddell Sea as it flows around the tip of the Peninsula and enters the strait (Heywood et al., 2004; Thompson et al., 2009; Sangrà et al., 2011; Zhou et al., 2002). Note that prior studies suggest there is no strong continuity between the AACC in the Weddell Sea and Bransfield Strait and the coastal current with the same name formed farther downstream in the Bellingshausen Sea (Moffat et al., 2008; Schubert et al., 2021). The northeastern path of the gyre is the Bransfield Current, which flows northeastward along the South Shetland Islands (Niiler et al., 1991;

Sangrà et al., 2011; Savidge & Amft, 2009; Zhou et al., 2002, 2006). The Bransfield Current is characterized by relatively warm and fresh water near the surface, and a ~10 km wide tongue of CDW below 300 m (Hofmann et al., 1996; Sangrà et al., 2011). Figure 1 shows a schematic of the circulation in Bransfield Strait and the northern cWAP. Two main water masses are found in Bransfield Strait resulting from the influences of the Bellingshausen and Weddell seas. Transitional Zonal Water with Bellingshausen influence (TBW) is relatively warm and fresh (García et al., 2002; Sangrà et al., 2011, 2017). Cold water (García et al., 2002; Hofmann et al., 1996; López et al., 1999; Sangrà et al., 2011; Tokarczyk, 1987) from the Weddell Sea forms Transitional Zonal Water with Weddell Sea influence (TWW, <0.2°C, 34.10 to 34.56). The cold TWW is the source for the waters found on the northern boundary of the SBF.

Despite being a critical feature of the hydrographic structure of the WAP shelf, the magnitude, temporal variability, and mechanisms of exchange between Bransfield Strait and the cWAP remain poorly understood. Studies based on summer observations have noted the flow from Gerlache Strait and across Bransfield Strait toward the South Shetland Islands (Niiler et al., 1991; Savidge & Amft, 2009; Zhou et al., 2002), as well as evidence of cold water from Bransfield Strait in Gerlache Strait (da Cunha et al., 2018; Parra et al., 2020), suggesting some degree of exchange across the SBF. Hydrographic time series collected in Andvord Bay revealed significant winter cooling in the deep layers (≥298 m) of that fjord, which were tentatively attributed to exchange with Gerlache Strait and local convection (Lundesgaard et al., 2020). In the cWAP, the conceptual model for the hydrographic structure described above is fundamentally two dimensional, with the lateral inflow of warm oceanic CDW being balanced by a combination of vertical mixing and melting processes at the coast (Couto et al., 2017; Klinck, 1998; Moffat & Meredith, 2018). Little attention has been given to what, if any, is the role of along-shore exchange in impacting the property budgets along the WAP, and how the structure of the front, and the exchange process across it, might evolve in time.

In this paper, we use the output of a state-of-the-art numerical model to investigate the variability and dynamics of along-shore water exchange in the WAP, and to understand how that exchange impacts the heat budget and thermal gradients along this region. We show that there is a significant seasonally-varying exchange of water between Bransfield Strait and the cWAP, with water of Weddell Sea origin flooding the southern shelf. We further show that the interannual variability in this exchange process is modulated by the Southern Annular Mode (SAM) through its influence on along-shore winds. Finally, we show that this process has a significant influence on the heat budget of the northern cWAP shelf, around Palmer Station. Available hydrographic data and supporting reanalysis products are also used to validate our findings and extend the temporal scale of the analysis. The model description, hydrographic data compilation, and ancillary data are described in Section 2. Results are shown in Section 3, and the implications are discussed in Section 4. Conclusions and a summary are included in Section 5.

2. Model Output and Available Data

2.1. High-Resolution Model Output

The ocean simulations were performed using the Regional Ocean Modeling System (ROMS), a free-surface, hydrostatic, terrain-following, primitive equation model (Haidvogel et al., 2008; Shchepetkin & McWilliams, 2005, 2009). The configuration includes a dynamical sea ice model (Budgell, 2005) as well as both mechanical and thermodynamic effects of static ice shelves, including melting (Dinniman et al., 2011; Holland & Jenkins, 1999). The model configuration used in this study was first introduced in Graham et al. (2016). The grid resolution is 1.5 km horizontally and has 24 vertical levels with an increased resolution near the surface and bottom (Shchepetkin & McWilliams, 2003, 2005). A realistic model bathymetry was generated using a combination of Bedmap2 (Fretwell et al., 2013) and the General Bathymetric Chart of the Oceans (GEBCO, 2008) dataset.

Open boundary and initial conditions for temperature and salinity include three sources: Monthly Isopycnal and Mixed-layer Ocean Climatology (Schmidtko et al., 2013) and World Ocean Atlas 2013 (WOA13, Locarnini et al. [2013]; Zweng et al. [2013]), and tagged seal profiles over the southern Bellingshausen Shelf (Graham et al., 2016). All these products were merged to provide the boundary and initial conditions for the model configuration (Graham et al., 2016). Velocity and sea surface height fields were obtained from the Simple Ocean Data Assimilation (SODA v2.2.4, Carton & Giese [2008]). Sea ice concentration boundary conditions were set using a combination of the Advanced Microwave Scanning Radiometer-Earth Observing System (AMSR-E, available up to October 2011) and Special Sensor Microwave Imager/Sounder (SSMIS, after October 2011).

For the first 2 months of the model run, all atmospheric forcing fields were obtained from the ERA-Interim produced by European Centre for Medium-Range Weather Forecasts (Dee et al., 2011). Starting on March 2006, the model was forced with atmospheric fields from the Antarctic Mesoscale Prediction System (AMPS; Bromwich et al., 2005; Powers et al., 2003, 2012) except for cloud fraction (not available in AMPS), which is from ERA-Interim (Dee et al., 2011). AMPS is an implementation of the Weather Research and Forecasting model (WRF) optimized for Antarctica, and provides mesoscale and synoptic atmospheric fields (Powers et al., 2012). Two versions of the AMPS data are used in the simulation with the resolution of 20 and 15 km, respectively. The temporal resolution used to force the ocean model is 6 hr for wind, and monthly for all other atmospheric forcing fields. An initial spin-up simulation was conducted from March 2006. In the model, dye representing the ice shelf meltwater, is initialized as zero everywhere and fluxed into the top layer of the model as a function of ice melt. Further details of the model configuration can be found in Graham et al. (2016).

2.2. Hydrographic Data

In order to evaluate the model, we compare the main statistics of the modeled and observed hydrographic properties both in the cWAP and Bransfield Strait (locations are shown in Figure 1b). Because these data are already included in the climatological averages used as boundary and initial conditions for the model, these comparisons do not provide a fully independent test of the model skill.

The first set of hydrographic measurements is from Autonomous Pinniped Bathythermograph (APB) data collected in February 2008 and included in the World Ocean Database 2013 (WOD13, Boyer et al., 2013). The second dataset is from the Palmer Long-Term Ecological Research project (PAL-LTER, Ross et al. [1996]; R. C. Smith et al. [2003]). We use the conductivity, temperature, and depth profiles from the 2008 cruise, which covers the grid lines from 200 to 600 (Figure 1b). In addition to this limited assessment of the model skill in the WAP, the hydrographic data collected at the PAL-LTER station 600.040 from 1993 to 2017 is also used to understand how the Weddell-sourced water impacts the deep water properties near Palmer Station (Figure 1b).

2.3. Ancillary Data

A number of ancillary datasets are used to characterize the impact of climate processes on WAP dynamics. These include monthly-averaged surface wind fields from ERA5 (Hersbach et al., 2020), provided on a $0.25° \times 0.25°$ resolution grid. There are also several climate indices used for analyses. Two important climate indices in the WAP region are the SAM and the El Niño/Southern Oscillation (ENSO), which will be used to understand the processes of interest here. The SAM is based on the average atmospheric pressure difference between a number of Antarctic and sub-polar stations, varies in interannual to decadal time-scales. The positive phase of the SAM index results in stronger westerlies over the WAP region (Marshall, 2003). ENSO is another primary climatic mode contributing to the variability of atmospheric circulation in the Southern Ocean. Yuan (2004) reveals that the La Niña event (negative ENSO) leads to a low-pressure system in the Amundsen-Bellingshausen Sea, which results in stronger northerly winds in this region. In this study, the observation-based SAM index is based on Marshall (2003) and the Oceanic Niño Index (ERSST.v5 SST anomalies in the Niño 3.4 region) was obtained from the National Oceanic and Atmospheric Administration (NOAA) Center for Weather and Climate Prediction.

3. Results

3.1. Model Validation

A comparison between the model output and available hydrographic observations for January 2008 is shown in Figure 2. The histograms show that modeled temperature and salinity agree well with the observations (Figures 2a and 2d). The vertical temperature structure reveals a warm bias in the model both in the surface the WW layers, with values of 0.1° near the surface and 0.5° from 50 to 100 m (Figure 2b). The simulated mean salinity profiles (Figure 2e) tend to differ from observations only near the surface, with a difference of around 0.1 (salinity in the PSS-78 scale, Figure 2e). Below 50 m, the model output captures the vertical structure of salinity well (Figure 2e). Both salinity ($r = 0.94$, $p < 0.01$) and temperature ($r = 0.81$, $p < 0.01$) mean profiles
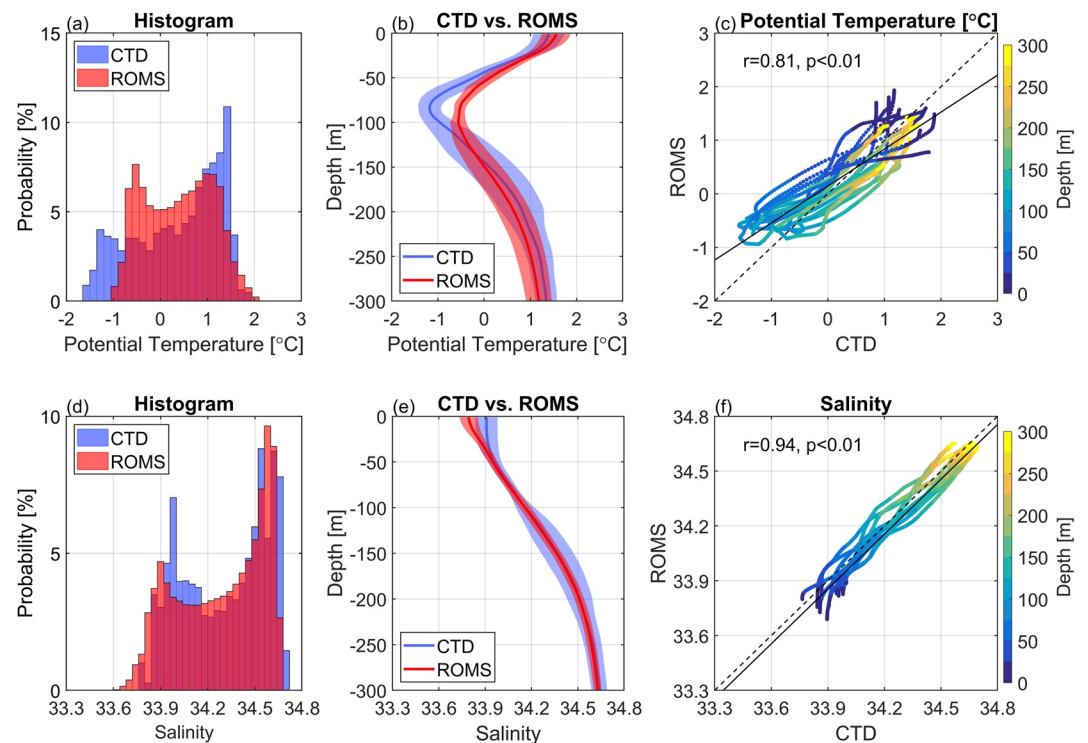
Figure 2. Comparison of observed and modeled potential temperature (°C, upper panels) and salinity (lower panels) for selected central West Antarctic Peninsula (cWAP) shelf stations (the locations of the stations are shown in Figure 1b). The observations are from January 2008 Palmer Long-Term Ecological Research project cruises, and the model output is averaged over that same month. (First column) Histograms of shelf profiles above 300 m. (Second column) Mean vertical profiles, the shaded area indicates the standard deviation of potential temperature and salinity. (Third column) Scatter plots for observed and modeled potential temperature and salinity, with color coded for depth. Dashed lines indicate the 1:1 relationship and solid lines are least-square regressions. A θ-S diagram for the cWAP shelf stations can be found in Figure S1 (supporting information).

are significantly correlated over the cWAP (Figures 2c and 2f). However, the observations show that the water column is well-mixed down to around 35 m (Figures 2c and 2f), whereas the mixed layer depth simulated by ROMS is relatively shallow compared to observations in summer (Figures 2b and 2e). The difference in the mixed layer depth between simulations and observations could have several causes. One possibility for the weaker mixing in the model is the lack of parameterization of Langmuir circulations, which impacts the intensity of vertical mixing (Schultz et al., 2020).

The comparison of model output and observations from February 2008 in Bransfield Strait (Figure 3b) reveals that the modeled temperature is colder than the observations in the upper 300 m. The cold bias maximum is 0.8°C near the surface and has another maximum of 0.6°C at 150 m, then decreases with depth (Figure 3b). For the salinity profile, the modeled salinity is around 0.25 fresher than the observations in the upper 150 m (Figure 3e). The bias of the salinity starts to decrease below 150 m, and the modeled salinity follows the structure of the observed salinity below 200 m closely. The fresher water near the surface is likely due to higher ice concentration in the model during the previous spring, which is caused by a delay in ice retreat (not shown). Despite these differences, the correlation between modeled and observed properties is high: $r = 0.80$ for temperature and $r = 0.81$ for salinity (both $p < 0.01$). Overall, the comparisons between the model and the limited available observations suggest that the model correctly represents the large along-shore hydrographic gradients of the WAP shelf. In Section 4, we expand on the need for further observational efforts to better characterize the SBF and validate modeling efforts in this region.
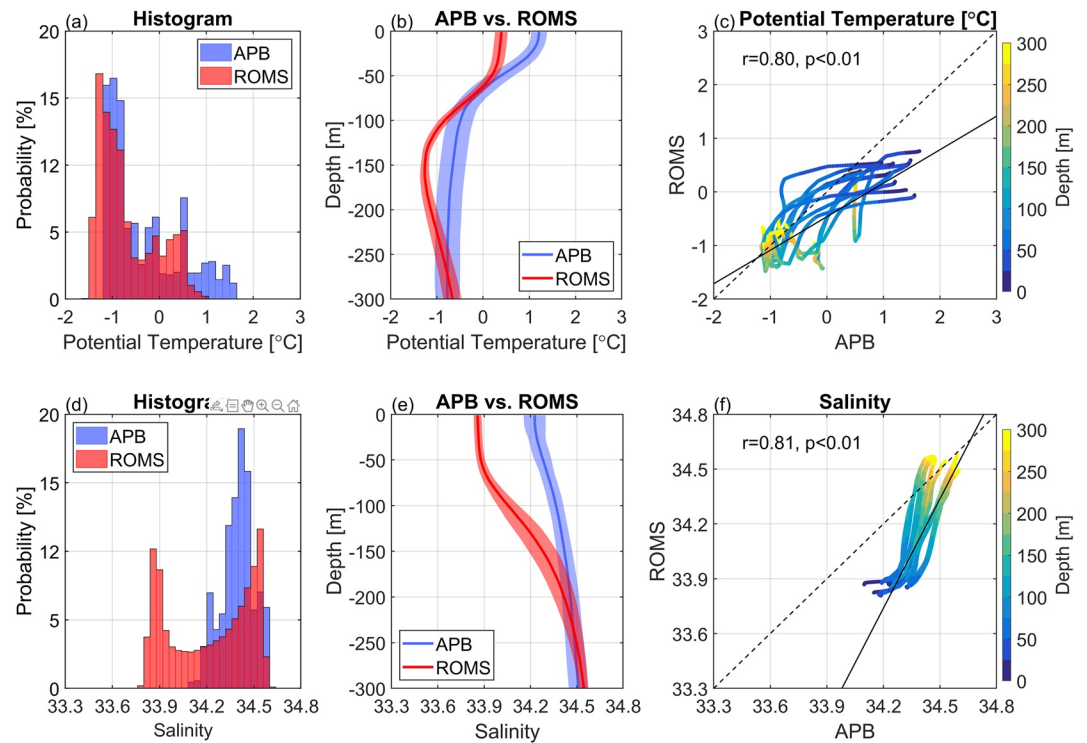
Figure 3. Same as Figure 2, but for Bransfield Strait stations (Figure 1b). The observations are the available Autonomous Pinniped Bathythermograph (APB) data from World Ocean Database 2013, collected in February 2008. A θ-S diagram for the Bransfield Strait stations can be found in Figure S1 (supporting information).

3.2. Seasonal Variations of Hydrographic Gradients and Exchange Along the WAP

3.2.1. Summer Hydrographic Properties and Along-Shore Exchange

Seasonal fields are calculated for summer (December/January/February) and winter (June/July/August). The modeled along-shore properties (Figures 4a–4g) reveal the structure of the SBF, separating the waters of Bransfield Strait from the cWAP (Moffat & Meredith, 2018). South of the front, the hydrographic structure is dominated by the three water masses of the cWAP (AASW, WW, and mCDW), while Bransfield Strait is occupied by TWW and TBW. Large differences in water mass structure are evident below 200 m (Figure 4). The potential temperature is typically >1°C below this depth in the cWAP, and <−0.5°C in Bransfield Strait (Figure 4a). A similar pattern is found in the salinity field (Figure 4c), with saltier water (>34.50) at depth to the south and fresher water to the north. The thermohaline gradients of this front are maximum at about 250 m, with a difference of about 1.7°C in potential temperature and 0.2 in salinity, over a spatial scale of around 30 km. The cross-shelf circulation (Figure 4e) associated with the SBF flows seaward at 0.1–0.2 m/s with a significant barotropic component. In summer, the SBF extends from the northern boundary of Gerlache Strait, across the island gaps between the cWAP and Bransfield Strait and across Boyd Strait (Figure 5a).

Horizontal maps of the seasonally-averaged potential temperature and velocity reveal two main pathways for the along-shore exchange of Weddell Sea water and mCDW during summer (Figures 5a and 5c). First, flow carrying cold water enters Bransfield Strait from the Weddell Sea, and largely flows cyclonically, with a small fraction of that flow entering Gerlache Strait and the gap between the coast and Low Island. Second, mCDW floods Bransfield Strait through the island gaps that separate it from the cWAP (Figure 5a). It moves offshore, retroflecting around Boyd Strait before mixing with CDW flowing into the Strait from the open ocean, forming a boundary current along the South Shetland Islands (Figure 5c).

The vertical structure of the along-shore exchange is illustrated with summer-averaged property and velocity sections across the island gaps between the coast and the shelf break (Figure 6, the locations of the sections are shown in Figure 1b). Both the hydrographic and velocity sections show narrow, bottom-trapped buoyant currents
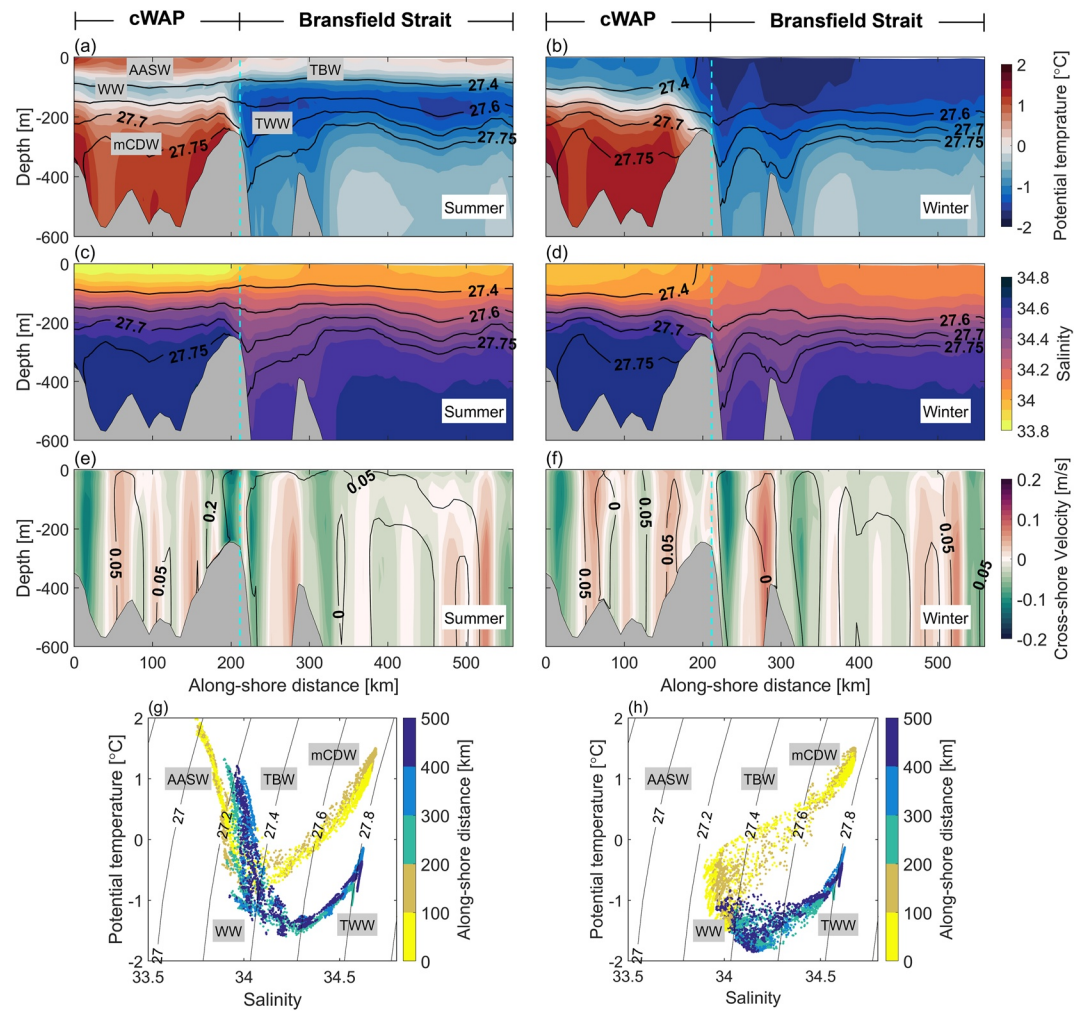
Figure 4. Seasonal-averaged circulation and hydrographic properties along the shelf (the location of the section is shown in Figure 1b) in summer (left panels) and winter (right panels) from the model output. Panels are (a), (b) potential temperature (°C) and (c),(d) salinity with isopycnals (potential density, kg/m³) overlaid, (e),(f) cross-shore velocity (m/s, positive velocity is toward West Antarctic Peninsula [WAP] shelf) with along-shore velocity contours overlaid. Panels (g), (h) show θ-S diagrams color coded for distance from the central WAP (cWAP) into Bransfield Strait. The cyan dashed line in panels (a)–(f) indicates the boundary that separates the cWAP from Bransfield Strait.

below 150 m in the gaps between the Peninsula coastline and Low Island, and Low Island and Smith Island (Figures 6a–6e). This incoming warm current has a potential temperature ranging from 0.5°C to 1.0°C and salinity ranging from 34.48 to 34.65. The steeply-tilted isopycnals indicate that the warm current near the shelf has a significant baroclinic component, which is formed by the density gradient between the cWAP and Bransfield Strait. The baroclinic Rossby radius of deformation is $r = \frac{NH}{f}$, where N is the buoyancy frequency, H is the vertical scale of the motion (~300 m near Low Island), and f is the Coriolis parameter ($f = 1.3 \times 10^{-4}\ s^{-1}$). $r = 10$ km near Low Island, which is consistent with the width of the current in Figure 6. The bottom-trapped currents have a typical velocity of 0.3 m/s.

Across Boyd Strait, a boundary current near Smith Island carries warm mCDW from the cWAP. Near the South Shetland Islands, a relatively warmer ($T_{max} \sim 1.4°C$) and saltier ($S_{max} \sim 34.70$) water with positive velocity circulates back to Bransfield Strait (Figures 6b–6f). This latter warm inflow through Boyd Strait has been observed near the South Shetland Islands in Bransfield Strait with the temperature above 1°C and salinity above 34.50 and identified as oceanic CDW (Hofmann et al., 1996; Sangrà et al., 2011, 2017). Our model analysis shows that mCDW from the cWAP also contributes to the narrow (≈12 km) deep warm current (0.30–0.40 m/s) along the
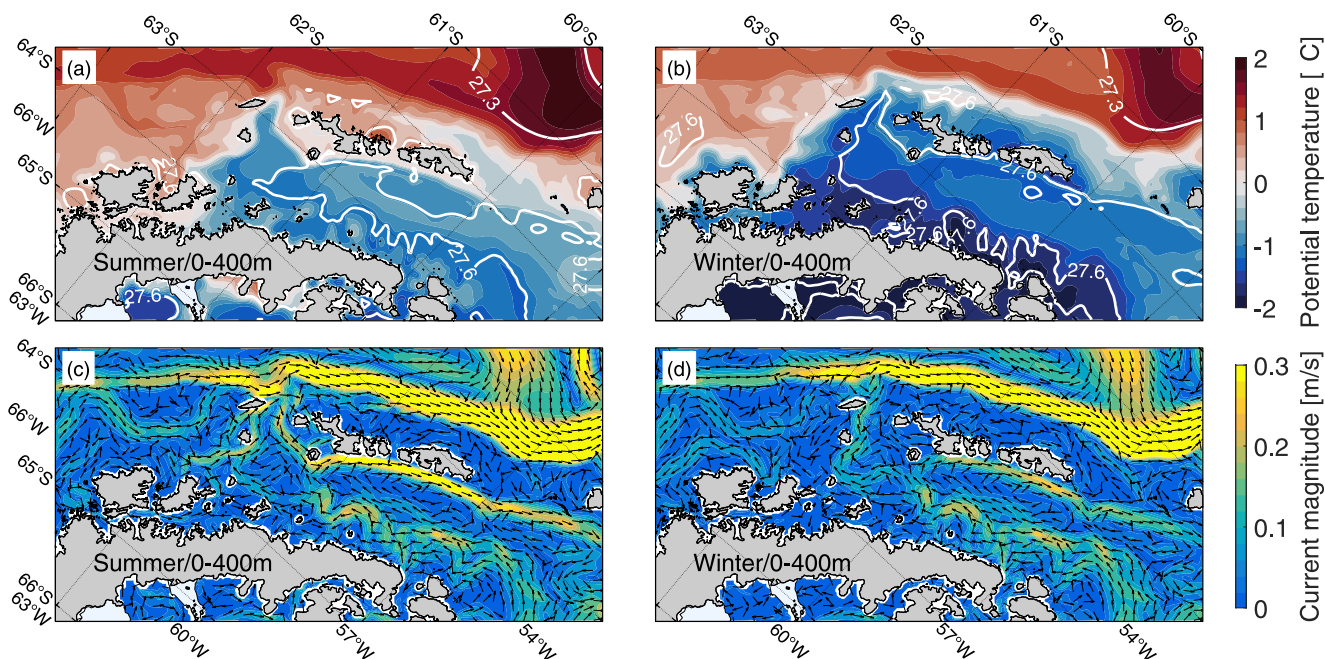
Figure 5. Summer (left panels) and winter (right panels) vertically-averaged (0–400 m) potential temperature and current from model simulations. (a), (b) Potential temperature (°C) and density (kg/m³, white contours). (c), (d) Current direction (arrows) and magnitude (m/s, color), sub-sampled every six grid points.
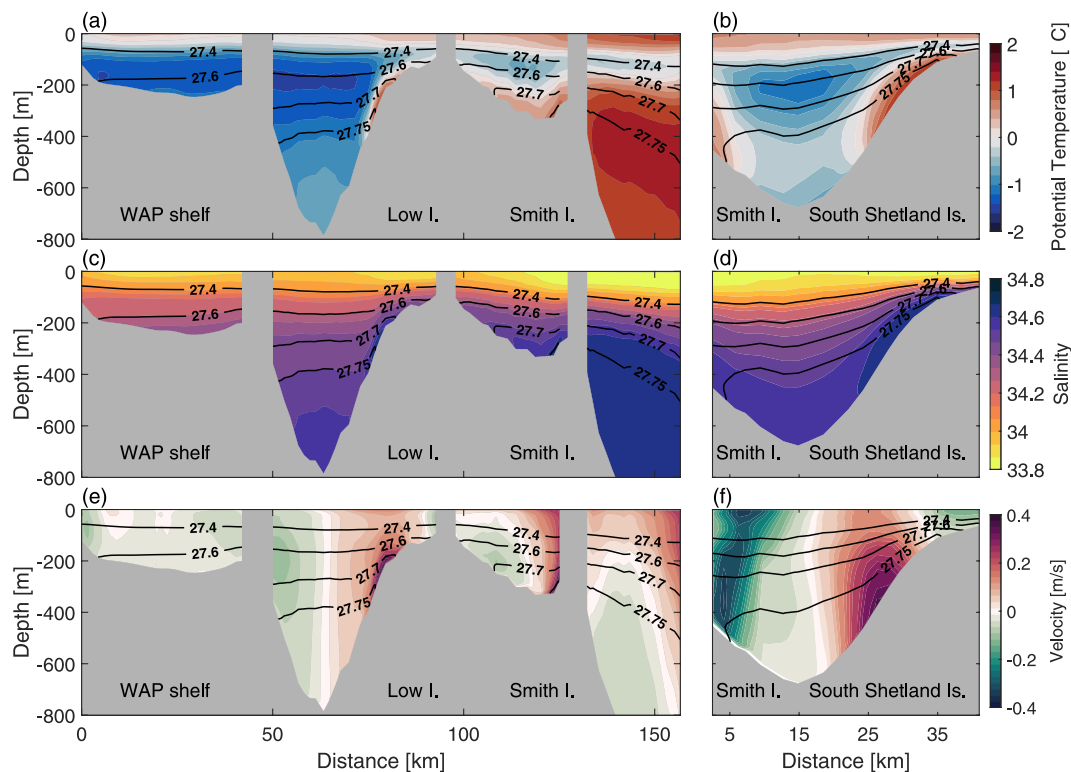
Figure 6. Summer-averaged ocean properties and velocity across the island gaps between Bransfield Strait and the central West Antarctic Peninsula, and across Boyd Strait (the locations of the sections are shown in Figure 1b). (a), (b) Potential temperature (°C) with isopycnals (kg/m³) overlaid. (c), (d) Same as panels (a) and (b), but for salinity. (e), (f) Same as panels (a) and (b), but for velocity perpendicular to the section (m/s, positive velocity is toward Bransfield Strait).
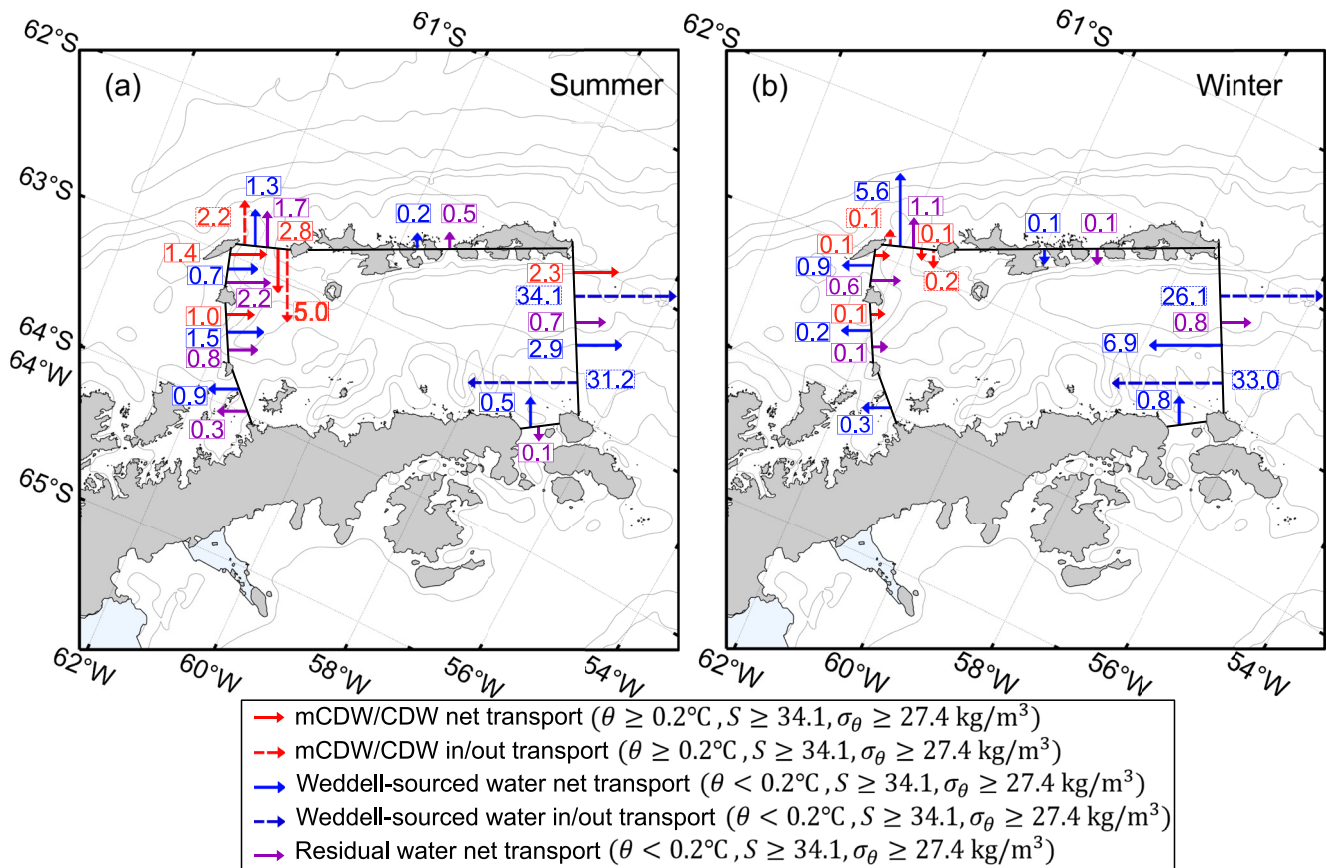
**Figure 7.** Schematic of the seasonal mass budget (in units of 10^5 m³/s) in Bransfield Strait for summer (a) and winter (b). The transports are labeled with red arrows for modified Circumpolar Deep Water (mCDW) and CDW, blue for the Weddell-sourced water, and purple for the residual volume flux. Solid arrows indicate the net transport of a water class (mCDW/CDW, Weddell-sourced, or residual) through a section, while dashed arrows indicate the transport of that water class entering/leaving Bransfield Strait. The arrows are scaled for visibility and do not match the relative transport sizes.

South Shetland Islands. mCDW recirculates back into Boyd Strait as a result of encountering the strong southern boundary of the Antarctic Circumpolar Current flowing along the shelf break (Figure 5c).

The summer-averaged mass budget shows the magnitude of the exchange along the shelf (Figure 7a). Note that this 2-year run does not represent a true climatological mean of this process. Based on the θ-S profile in Figures 4g and 4h and the cross-section water properties in Figures 6 and 8, we use the $\sigma_\theta = 27.4$ kg/m³ and $S = 34.1$ to separate the Weddell-sourced water and the relatively fresher and lighter residual water masses (AASW, WW, and TBW). Considering the presence of the mCDW/CDW core in the deep layers in Bransfield Strait, the criteria to identify Weddell-influenced water and mCDW/CDW are as follows: mCDW/CDW dominated water masses are defined as $\sigma_\theta \geq 27.4$ kg/m³, $S \geq 34.1$, and $\theta \geq 0.2$°C. Water with $\sigma_\theta \geq 27.4$ kg/m³, $S \geq 34.1$, and $\theta < 0.2$°C is classified as Weddell-sourced water in the mass budget. We thus capture the seasonal cycle of the along-shore water exchange with a focus on Weddell-sourced water and mCDW/CDW.

Near Low and Smith islands, the inflow of mCDW is evident in the northeastward transport across the island gaps (Figure 5c), with a net transport of 2.4×10^5 m³/s (Figure 7a). Once this boundary current reaches Boyd Strait, the mCDW being transported therein mixes with CDW entering Bransfield Strait from the open ocean and then recirculates into Bransfield Strait and along the South Shetland Islands. The inflowing transport is around 5.0×10^5 m³/s (Figure 7a). The water exchange of mCDW and CDW in Boyd Strait suggests that around 44% of the warm water found near the South Shetland Islands is contributed from mCDW in the cWAP. This is notable because, while several previous studies have characterized this warm subsurface current (e.g., Barlett et al., 2018; Dotto et al., 2021; Hofmann et al., 1996; Sangrà et al., 2017, 2011; Zhou et al., 2006), how much the mCDW from the northern cWAP contributes to its formation was not known.
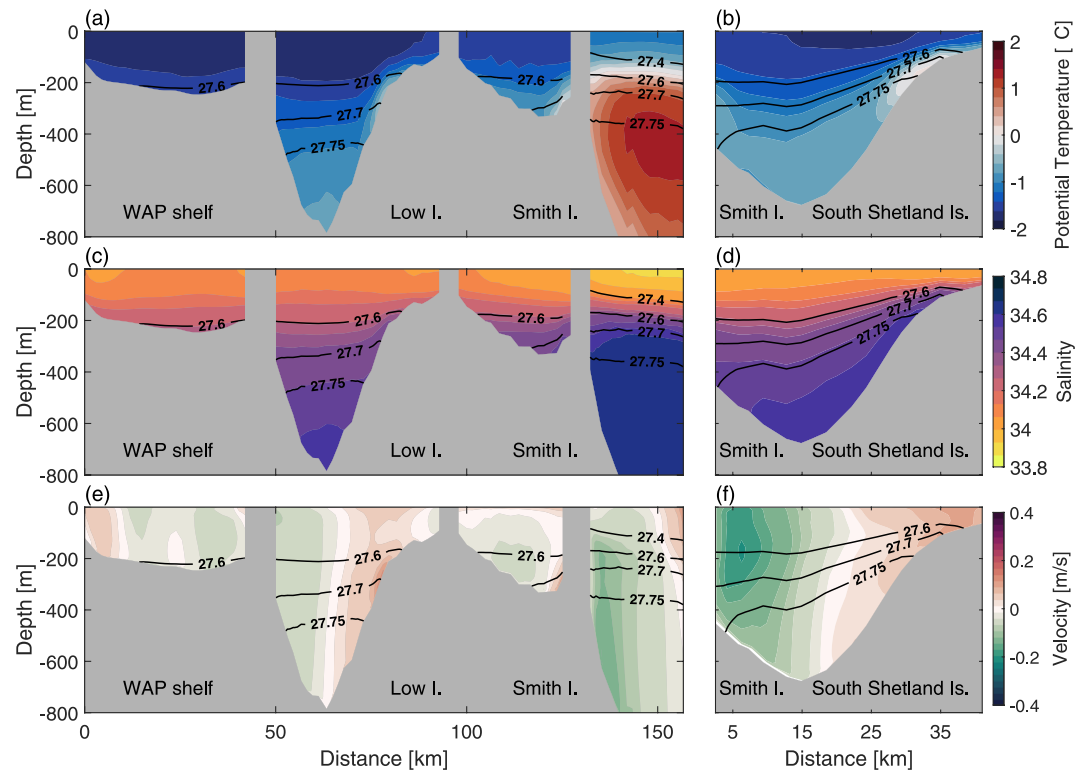
Figure 8. Same as Figure 6, but for the winter mean ocean properties and cross-section velocity.

The summer-averaged model output shows 31.2×10^5 m³/s of Weddell-sourced water entering Bransfield Strait, of which about 21.0×10^5 m³/s corresponds to the transport within the AACC (integrated above 27.75 kg/m³ isopycnal of northern boundary in Bransfield Strait). This is consistent with values of $24.0 \pm 10.0 \times 10^5$ m³/s from observational (von Gyldenfeldt et al., 2002) and 20.0×10^5 m³/s from modeling studies (Jiang et al., 2013). The largest inflow of cold water from Bransfield Strait to the cWAP (0.9×10^5 m³/s) occurs through Gerlache Strait. A perhaps counterintuitive result is the summer inflow of cold Weddell-sourced water through the island gaps (1.5×10^5 m³/s and 0.7×10^5 m³/s). This can be readily understood as the result of remnants of cold water on the cWAP from prior flooding being advected back to Bransfield Strait. This mechanism is discussed in more detail in the next section.

3.2.2. Winter Inflow From Bransfield Strait to the cWAP

The flow from the Weddell Sea follows distinct pathways in Bransfield Strait during the winter relative to the summer, leading to a significantly larger cold inflow to the cWAP (Figures 5b and 5d). As cold Weddell-sourced water moves cyclonically around the strait, enhanced inflow into the cWAP is generated via Gerlache Strait and the gaps between the Peninsula coastline, Low Island, and Smith Island (Figure 8). A second pathway for exchange forms as cold water overflows from Bransfield Strait onto the shelf break through Boyd Strait, remaining largely trapped to the bottom as it flows around Smith Island, and eventually reentering the cWAP. The cross-shore sections (Figure 8) show a weakly bottom-intensified flow on the shelf break off Smith Island, which is transporting colder water there before reentering the shelf. Correspondingly, the intrusion of mCDW/CDW is weaker in winter, and the hydrographic properties in this exchange region (i.e., island gaps and Gerlache Strait) are dominated by cold water from the Weddell Sea (Figure 5b). This is evident in the reversal of the flow near the coast and the reduction or disappearance of the warm inflow through the island gaps.

The summer-to-winter transition described above results in changes in the location and structure of the Southern Bransfield Front (SBF). In Bransfield Strait, the incoming Weddell-sourced waters in the upper 400 m are −1.9°C to −1.4°C compared to −1.2°C to −0.5°C during summer (Figures 5a and 5b). In the cWAP, meanwhile, the surface waters experience cooling to about 150 m (Figure 4b). The vertically-averaged potential temperature in Gerlache Strait and the island gaps decreases from 0.5°C in summer to −0.8°C in winter (Figures 5a and 5b)
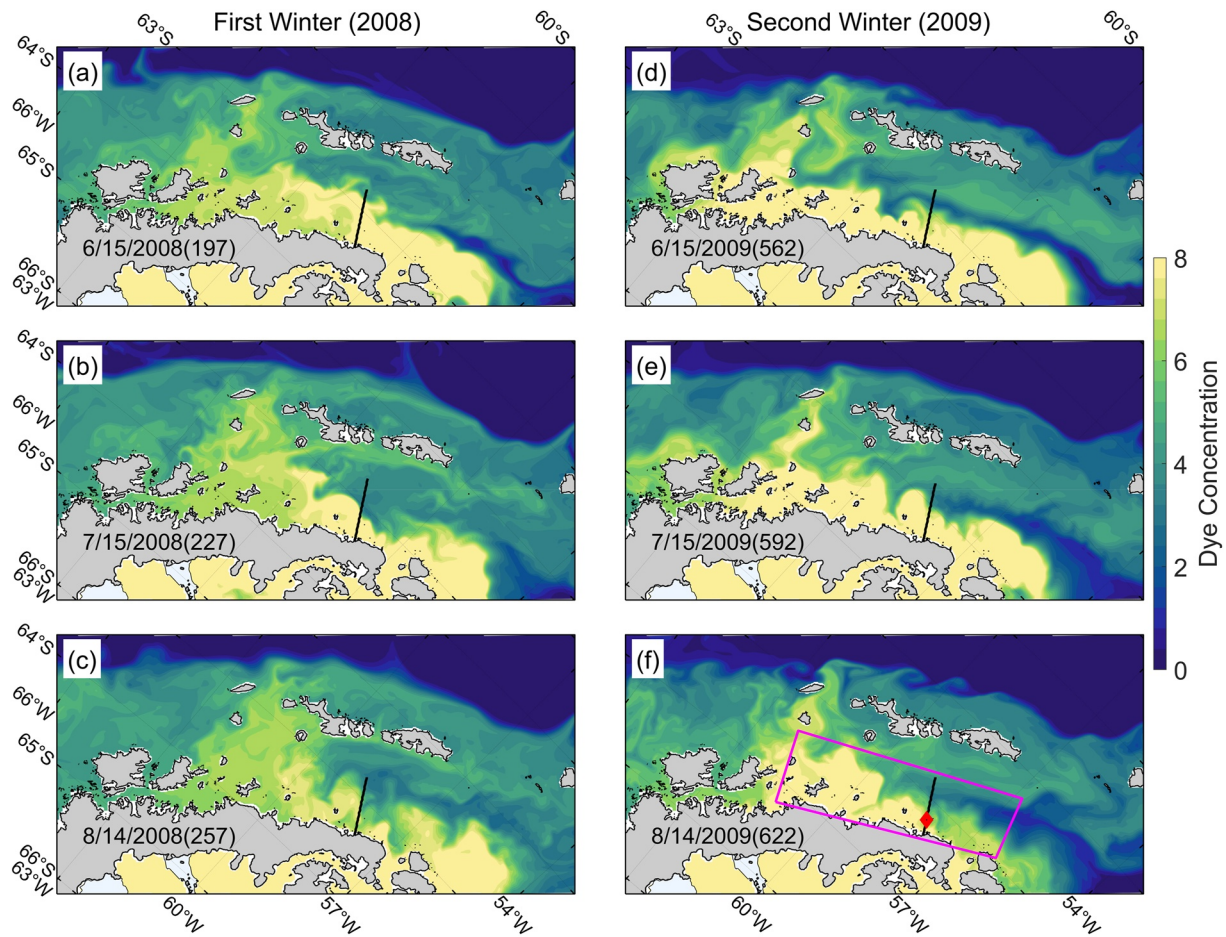
Figure 9. Surface dye concentration (ice shelf meltwater) in the first winter (left column) and second winter (right column). Each plot shows the instantaneous output of that day. The black line in all panels is the cross-shore section of Figures 10b and 11. The red diamond in panel (f) is the location of Figure 10c, and the magenta box shows the domain for calculating the average wind stress.

as the surface cools and Weddell Sea Water is advected southward. The SBF (here defined as the location of the 0°C isotherms in Figure 5) migrates around 25 km south of the island gaps as a result. In Gerlache Strait, the SBF is found near the northern end in summer (Figure 5a) and moves to the the southern end in winter (Figure 5b).

While the inflow from the Weddell Sea is colder during the winter, the mass budget in Bransfield Strait (Figure 7b) reveals only a relatively small increase of 2.1×10^5 m³/s (6.6%) in the volume transport of that water from the Weddell Sea. Instead, the key difference is in its fate in Bransfield Strait. Around 26.1×10^5 m³/s of the inflow circulates through the Bransfield Strait before exiting along the South Shetland Islands in winter. The net flux of the Weddell-sourced water flooding the cWAP increases by 7.0×10^5 m³/s in winter compared to summer. At the same time, the total flux of mCDW/CDW into Bransfield Strait decreases from 5.2×10^5 m³/s in summer to 0.3×10^5 m³/s in winter. Overall, the direction of along-shore exchange largely reverses in winter, with a net flux of cold Weddell-sourced water toward the cWAP.

3.3. Interannual Variability and Wind-Modulated Flow in Bransfield Strait

As shown above, the model reveals that the cold water from Bransfield Strait floods into the cWAP via Gerlache Strait and the island gaps during the winter (Figure 7). To better understand the dynamics of the intrusions, we examine the characteristics of the Weddell-sourced water flowing along the Peninsula coastline during the winter. The model was set up to dye ice shelf meltwater, which results in this output being a good proxy for the Weddell Sea inflow to the WAP. Figure 9 shows snapshots of the evolution of the intrusions to the WAP in the two modeled winters. During the first winter (Figures 9a–9c), a large portion of the intruding cold water separates

from the Peninsula coast after entering Bransfield Strait, with little flooding of cold water toward the cWAP. In contrast, the Weddell Sea inflow remains trapped against the Peninsula coastline in Bransfield Strait during the second winter (Figures 9d and 9e), and a relatively large amount of this cold water floods into the cWAP via Gerlache Strait and the island gaps (Figure 9f). Drifter trajectories (Renner et al., 2012) suggest that the advective pathways of the water originated from the Weddell Sea are influenced by wind-forcing.

The structure of the inflow from the Weddell Sea in Bransfield Strait suggests that wind forcing plays a significant role in either advecting the inflow off the coast or keeping it trapped against the coast of the Peninsula. The large differences in the flow structure between the two winters imply that while the intrusions occur seasonally, their impact on the cWAP varies significantly in interannual timescales. We emphasize that the relatively short model run we are analyzing here is unlikely to capture the full breadth of interannual variability of this system. However, our analyses reveal important dynamics of the along-shore exchange process, which we examine below.

3.3.1. The Response of Intruding Weddell Sea Water to Along-Shore Wind Forcing

The structure and variability of wind forcing along the WAP shelf are heavily influenced by the orientation and latitudinal extent of the Peninsula with respect to the westerlies flowing around Antarctica. Offshore, the winds are blowing roughly toward the main axis of the Peninsula, and as they reach it, they split into a northern branch flowing northwards along the coast of Bransfield Strait and a southward-flowing branch along the cWAP south of Anvers Island. On average, the winds tend to be upwelling-favorable along the Bransfield Strait coast and downwelling-favorable along the cWAP (Van Lipzig et al., 2004; van Wessem et al., 2015). The AMPS wind fields used to force the model are consistent with the above description (Figure 10a), showing that the mean wind stress along Bransfield Strait is predominantly northeastward along the coast, that is, upwelling-favorable.

To investigate the role of wind forcing on the dynamics of the intruding Weddell Sea water in Bransfield Strait, we examined the impact of both along-shore winds as well as of wind curl over Bransfield Strait. Both forcings have the potential to modulate the cross-shore structure and along-shore transport of the Weddell Sea inflow. First, the daily wind stress output was rotated into along- and cross-shore components. Then, spatially-averaged values for both the along-shore wind stress and Ekman pumping velocity were calculated for the region shown in Figure 9f (magenta box). To compare both forcings, area-averaged estimates of Ekman pumping ($w = \hat{k} \frac{1}{\rho f} \nabla \times \tau$, i.e., upwelling driven by wind curl) and of upwelling driven by the along-shore winds were calculated.

During the first winter, the along-shore wind is relatively more upwelling-favorable, with a mean of 0.021 N/m². The wind stress reverses direction to downwelling-favorable starting in the second fall. During the second winter, the along-shore wind stress has a mean of 0.004 N/m² and is more variable, with overall weaker upwelling-favorable wind events and several large downwelling-favorable wind events. The Ekman pumping velocity closely follows the wind stress variability, with a significant cross-correlation of 0.60 ($p < 0.01$, Figure 10a). Positive Ekman pumping (upwelling favorable) is dominant during the first winter, with more variable values during the second winter. Both the wind stress and the Ekman pumping contribute significantly to upwelling and downwelling close to the WAP coast. The average vertical velocity as a result of Ekman pumping contributes about 36% of the total wind driven upwelling in the first winter and it is of similar magnitude as the along-shore wind-driven component during the second winter. Although Ekman pumping can be stronger in some events, wind-driven upwelling is typically larger. The high temporal correlation between these two mechanisms suggests wind stress can be used as a reliable proxy for the modulation of wind effects on the along-shore transport in Bransfield Strait.

The impact of the interannual variability of wind on the properties of the incoming flow from the Weddell Sea is illustrated in Figures 10b and 10c. As expected from previous work on coastal current response to wind forcing (e.g., Lentz, 2004; Moffat & Lentz, 2012; Sutherland & Pickart, 2008), as the winds become consistently upwelling-favorable in the first winter, and occasionally in the second winter, the plume widens (Figure 10b) and becomes shallower (Figure 10c) as Ekman transport pushes the surface water offshore and there is compensating upward movement at depth. The salinity field shows the intruding cold water spreads around 60–80 km away from the WAP shelf (Figure 10b). In the mid-spring of the first year, the cross-shelf area of the coastal plume narrows to about 20 km after the wind decreases. When the wind reaches another relative maximum in late spring, the cold water outflow widens again in Bransfield Strait (Figure 10b). The vertical structure (Figure 10c) is again consistent with the surface changes, showing the uplift of the deep isopycnals along the bottom from about 500 to 300 m. During the more variable conditions of the second year fall and winter, the 34.30 isohaline (white contour)
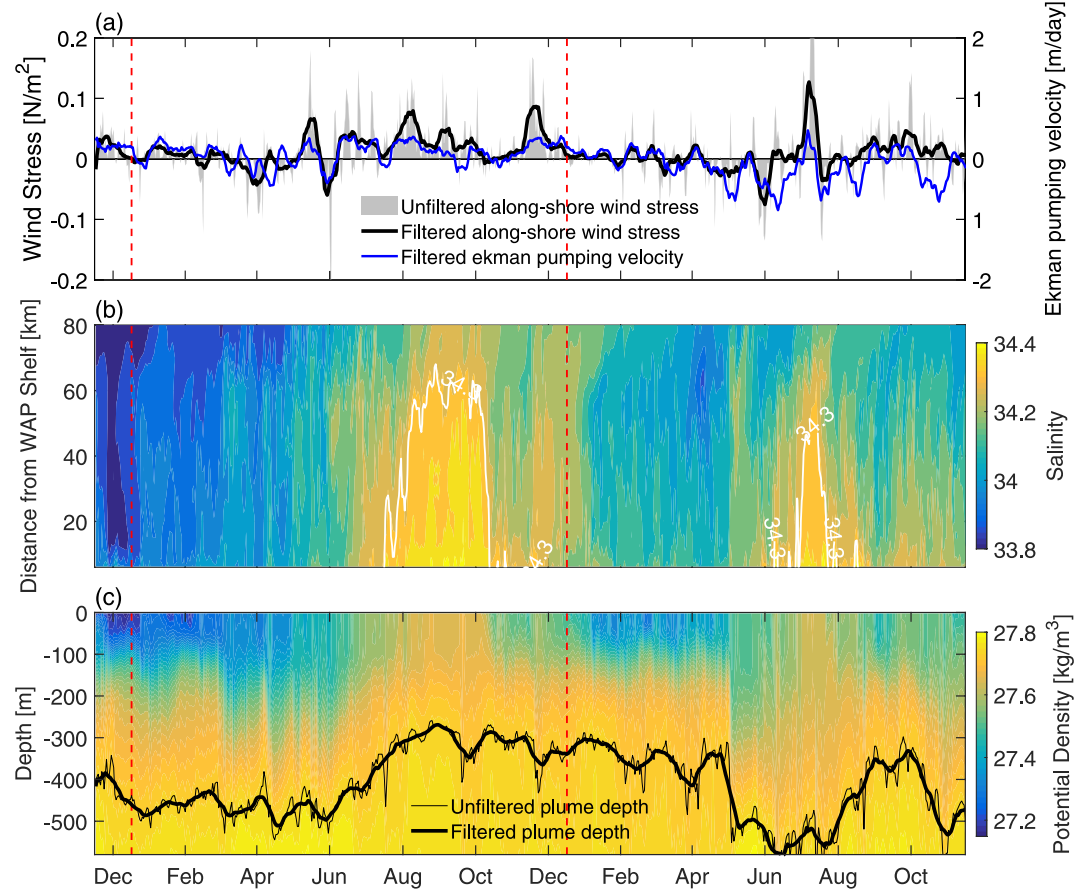
Figure 10. (a) Time series of along-shore wind stress (N/m², the along-shore direction is about 61.07° east of north) and Ekman pumping velocity (m/day) in Bransfield Strait (the domain used to average both is shown in Figure 9f). (b) Depth-averaged (0–50 m) salinity of the cross-shore section in Bransfield Strait (the location of the section is shown in Figure 9). The width of the surface current is defined by the 34.30 isohaline, highlighted in white. (c) Potential density (kg/m³) versus depth at a single point on the cross-shore transect (the location is shown in Figure 9f). The black line indicates the buoyant plume depth as defined by the 27.75 kg/m³ isopycnal. The red dashed lines in all panels separate years 2008 and 2009. The thick lines in panels (a) and (c) have been smoothed using a 15-day running mean.

is not observed when the wind is downwelling-favorable. When the wind reverses to upwelling-favorable for a relatively short period in July of 2009, the current widens to about 60 km again.

Our results show the along-shore wind stress strongly modulates the structure and transport of the coastal current along the WAP shelf (Figure 11). In addition to the changes in the cross-shore hydrographic structure discussed above, the along-shore velocity increases during the second winter, as a result of the steepening isopycnals intensifying the geostrophic shear (Figures 11c and 11f) combined with enhanced cross-shore surface elevation slope increasing the barotropic transport (not shown). The along-shore wind stress and along-shore volume flux (integrated above the 27.75 kg/m³ isopycnal, Figure 12) are significantly correlated. The upwelling-favorable conditions during 2008 resulted in diminished along-shore transport compared to the more variable wind conditions of 2009 when the mean along-shore wind stress is about 0.02 N/m² smaller than in 2008. The resulting along-shore transport increases by an average of 1.6×10^5 m³/s. Overall, the changing wind forcing conditions during the two winters appears to be the leading cause for the interannual variability of the coastal current structure and transport along the WAP. Downwelling-favorable wind favors along-shore propagation of the plume along the coast, resulting in enhanced flooding of the cWAP by cold Bransfield Strait water.

3.3.2. Links to Climate Indices

The analysis presented above suggests local wind forcing drives important interannual differences in the magnitude of along-shore water intrusions from Bransfield Strait to the cWAP. Wind patterns are strongly modulated
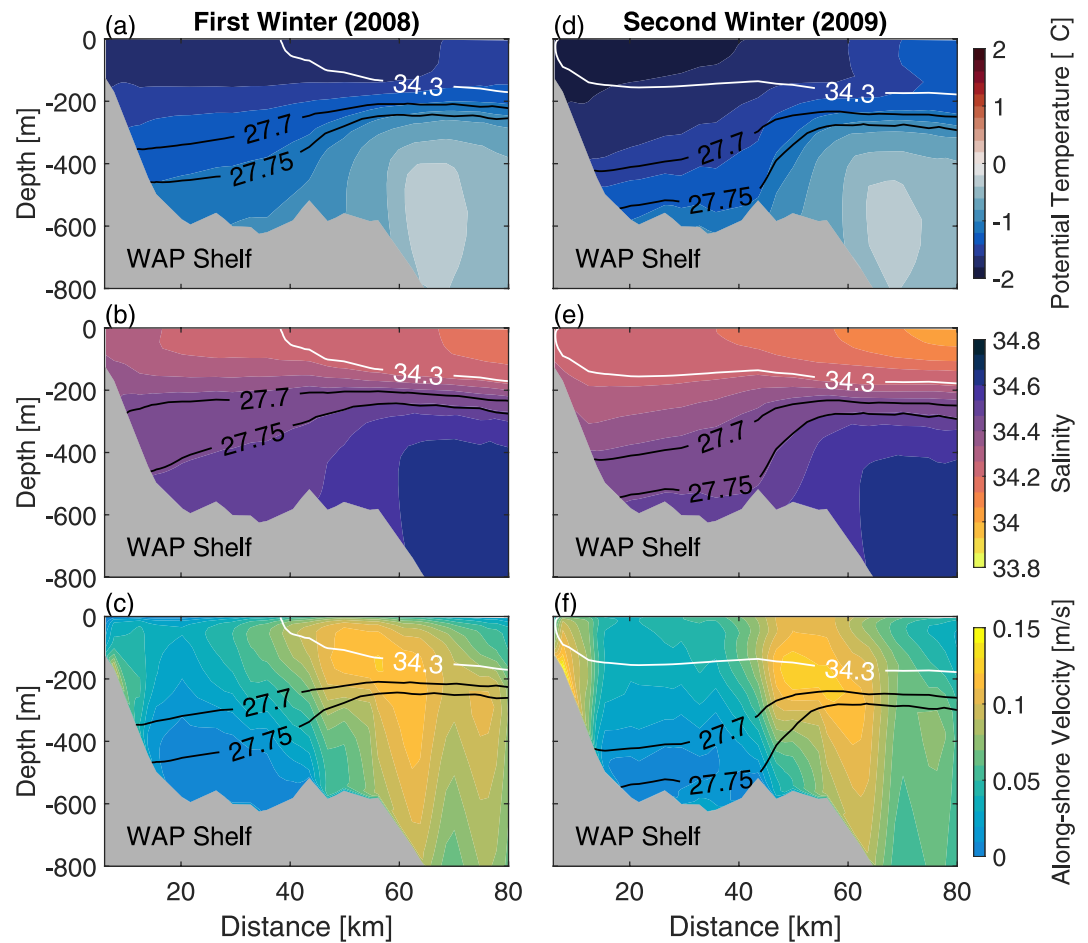
Figure 11. Winter-averaged hydrographic properties and velocity of the cross-shore section (the location of the cross-shore transect is shown in Figure 9) in 2008 (left panels) and 2009 (right panels). (a), (d) Potential temperature (°C) field of the cross-shore section with isopycnals (kg/m³) overlaid, the 34.30 isohalines are also highlighted in the two panels. (b), (e) Same as panels (a) and (d), but for the salinity field. (c), (f) Same as panels (a) and (d), but for along-shore velocity (m/s), positive velocities indicate flow toward the southwest.

by climate modes over the WAP (e.g., Dotto et al., 2016; Meredith et al., 2017), including the SAM and ENSO. Along-shore wind stress in Bransfield Strait flows largely in the E-W direction and is therefore dominated by the intensity of the westerlies near the WAP shelf. Our short model run does not allow us to fully evaluate the impact of SAM/ENSO variability on ocean processes. Instead, we use ERA5 wind fields from 1979 to 2017 to estimate the modulation of SAM and ENSO on winds in Bransfield Strait. ERA5 winds match closely with the AMPS winds used to force the model (Figure S2, supporting information). We mainly focus on the period from late fall to early spring because the simulations show that this is when Weddell-sourced water is flooding the cWAP.

Figure 13 shows the mean, winter-averaged along-shore wind stress and corresponding SAM and ENSO indices. The cross-correlation of the along-shore wind stress in Bransfield Strait and the SAM index is 0.45 ($p < 0.01$) at zero time lag (Figure 13a), while the correlation with the ENSO index is smaller ($r = 0.17$, Figure 13b) and not significant at the 95% level. This implies that a positive phase of SAM in winter is correlated with the up-welling-favorable wind (stronger westerlies) along the peninsula coast of Bransfield Strait, driving the coastal current offshore and reducing the magnitude of the flooding of the cWAP. The opposite occurs during the nega-tive SAM phase, which leads to the weaker upwelling-favorable wind to the downwelling-favorable wind (weaker westerlies) in Bransfield Strait, resulting in forcing conditions that favor intrusion of the coastal current to the cWAP. We note that some years (e.g., 1998) are inconsistent with the stated influence of SAM over the along-shore winds, and this might reflect the influence of significant ENSO events and its teleconnection with SAM. Previous studies have shown that during La Niña events, the depth of the Amundsen Sea Low (ASL) deepens
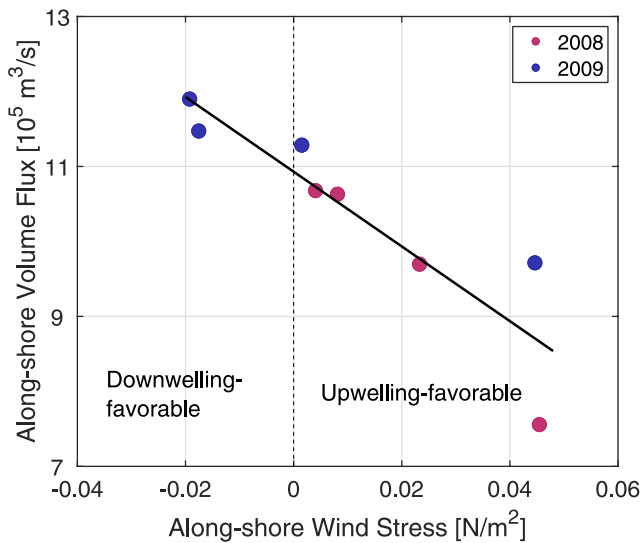
Figure 12. Along-shore volume flux along the Bransfield Strait versus along-shore wind stress. The volume flux is integrated above 27.75 kg/m³ isopycnal of the cross-shore section in Figure 11, with positive values indicating flux toward the southwest. Positive wind stress is upwelling-favorable. Both the flux and wind stress are monthly-averaged for May, June, July, and August in year 2008 (Red dots) and 2009 (blue dots). The thick line is a linear fit.

(Clem & Fogt, 2013; Turner et al., 2013). Fogt et al. (2011) also noted that when a La Niña event occurs with positive SAM, it could have a strong impact on the atmospheric circulation in a region extending from the central Pacific to the Amundsen-Bellingshausen Sea. The resulting lower pressure in the ASL could generate a stronger north to northwesterly wind over the WAP. This may be the reason for the observed variability in 1998.

### 3.4. Impacts From Along-Shore Exchange on the Ocean Properties and Heat Budget in Northern cWAP

Previously, the heat budget in the cWAP has been conceptualized as mainly two-dimensional (Couto et al., 2017; Klinck, 1998; Moffat & Meredith, 2018), without considering the along-shore heat transport as a significant component. Our results suggest that at least in the northern cWAP, seasonal flooding of cold water from Bransfield Strait plays an important role in the heat budget. To evaluate this hypothesis, we compute each term of the heat budget using the diagnostic output from ROMS:

$$\rho C_p \frac{\partial \theta}{\partial t} = \rho C_p \left(\frac{\partial u\theta}{\partial x} + \frac{\partial v\theta}{\partial y} + \frac{\partial w\theta}{\partial z} \right) + \rho C_p \left(\frac{\partial}{\partial z} \left(\kappa_V \frac{\partial \theta}{\partial z} \right) \right. \\ \left. + \nabla_H \cdot (\kappa_H \nabla_H \theta) \right) \tag{1}$$

The above terms were integrated from 200 m to the bottom over the cWAP (see box in Figure 1b) to focus on the competition between the cold Bransfield Strait inflow and the warm inflow from the Bellingshausen Sea. Here, θ is the potential temperature, C_p is the heat capacity, ρ is a reference density, (u, v, w) are the velocity components, and κ_V and κ_H are the turbulent vertical and horizontal diffusivity coefficients, respectively. The three terms on the right, modulating the variability of the heat content, represent the horizontal and vertical heat flux divergence and the diffusive heat flux, respectively.
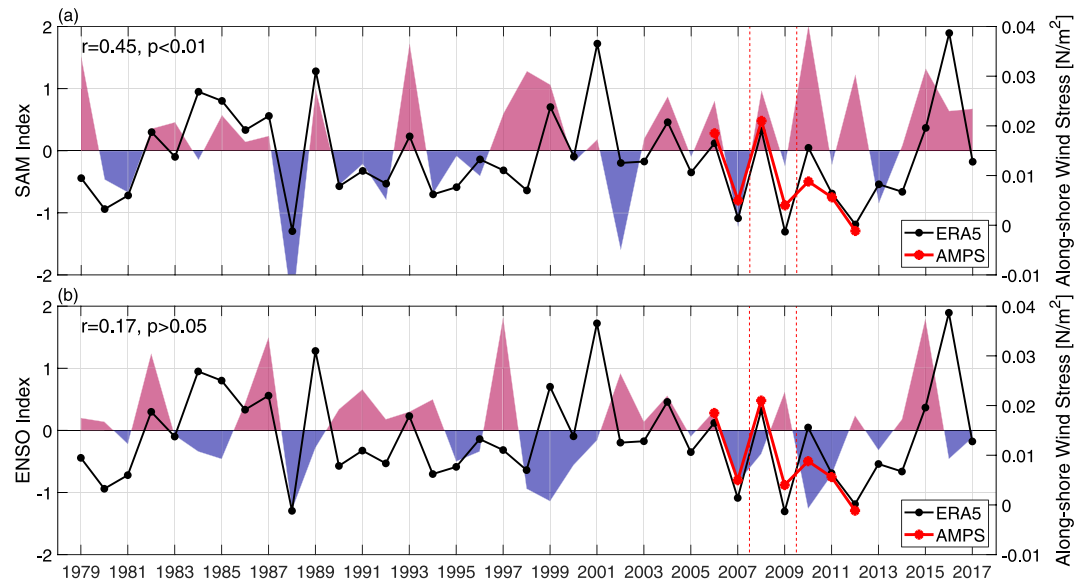
Figure 13. (a) Time series of the Southern Annual Mode (SAM) index and along-shore wind stress ($r = 0.45$, $p < 0.01$) from 1979 to 2017. Positive SAM is illustrated in red, negative ones are in blue. The dotted thick red line is the winter-averaged along-shore wind stress from model forcing Antarctic Mesoscale Prediction System (AMPS, 2006-2012). The dotted thick black line is the winter-averaged along-shore wind stress, which is calculated from ERA5 wind fields (the same domain in Figure 9f). A comparison between the monthly-averaged along-shore wind speed from AMPS and ERA5 can be found in Figure S2 (supporting information). (b) Same as panel (a), but for the oceanic Niño index ($r = 0.17$, $p > 0.05$). The red dashed lines in both panels indicate the model time domain (2008-2009).
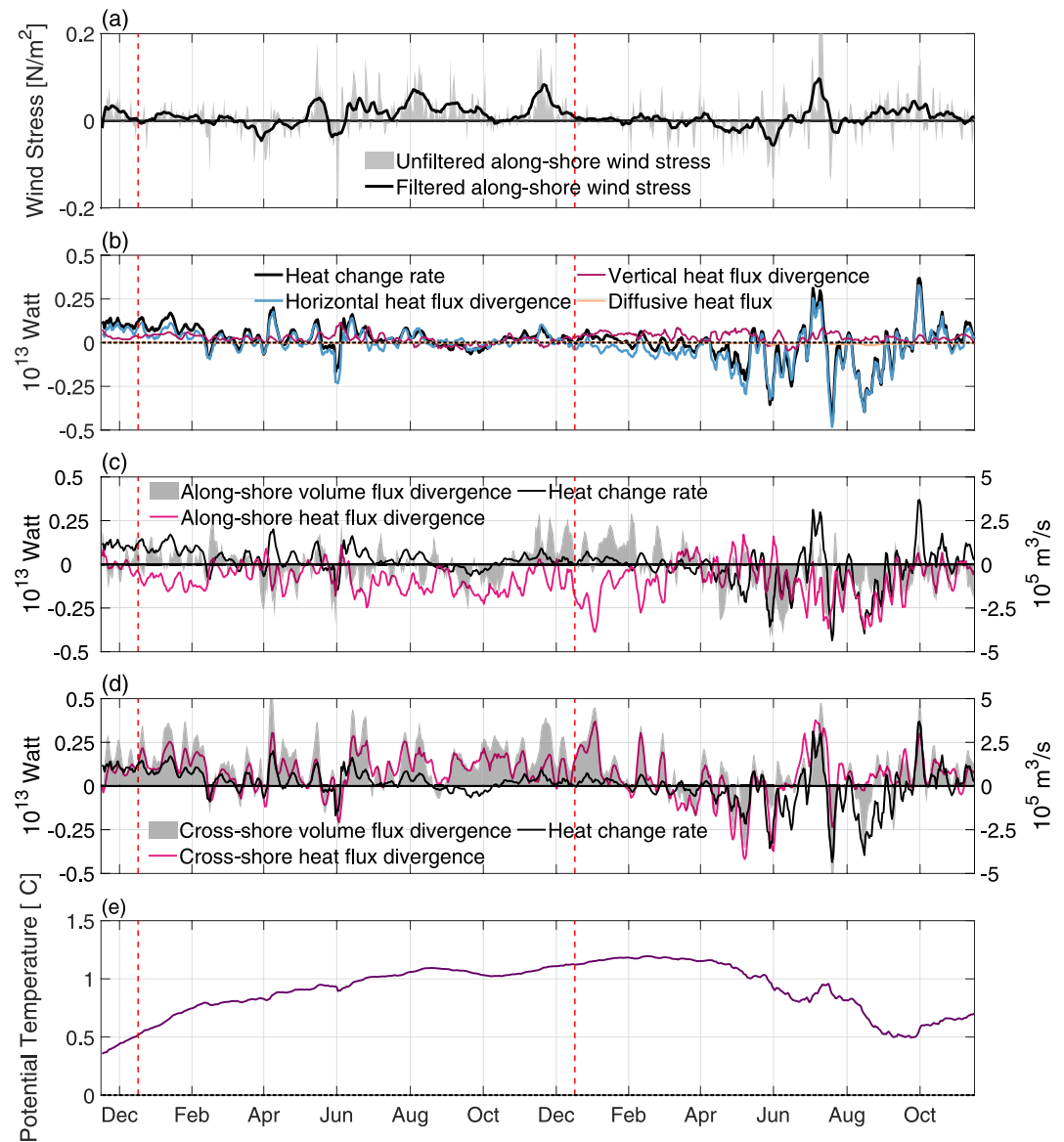
Figure 14. (a) Time series of along-shore wind stress (N/m²) in Bransfield Strait (same as Figure 10a). (b) Time series of the integrated terms in heat budget Equation (1). (c) Along-shore volume flux divergence (10^5 m³/s) and heat flux divergence (10^{13} W). (d) Same as panel (c), but for the cross-shore direction. (d) Mean potential temperature (°C). In panels (b)–(d), positive values mean warming and increasing volume. The time series in panels (b)–(d) have been smoothed using a 5-day running mean. The red dashed lines in all panels separate years 2008 and 2009.

Consistent with the exchange mechanisms discussed above, the analysis of the heat budget shows that the impact of the cold water intrusion is significant, especially during the second winter. Figure 14e reveals that there is a steady increase in the deep temperature during the first half of the simulation, a result of inflow of heat from the open ocean, and there are only a few weak reversals in this trend, with at least one associated with a strong downwelling-favorable wind event in June of 2008. The deep temperature is around 1°C during the first winter and drops more than half a degree during the second fall to winter (Figure 14e), which is consistent with the negative horizontal heat flux divergence in the northern cWAP (Figure 14b) and the reduction of heat supply from the open ocean (Figure 14d). This latter effect is consistent with a reduction of the wind intensity over the northern cWAP resulting in reduced CDW inflow to the shelf (Dinniman et al., 2012). The above analysis shows that along-shore exchange can have a significant impact on the heat budget in the northern cWAP region around Palmer Station. Downwelling-favorable winds that are more prevalent during years where the SAM index is
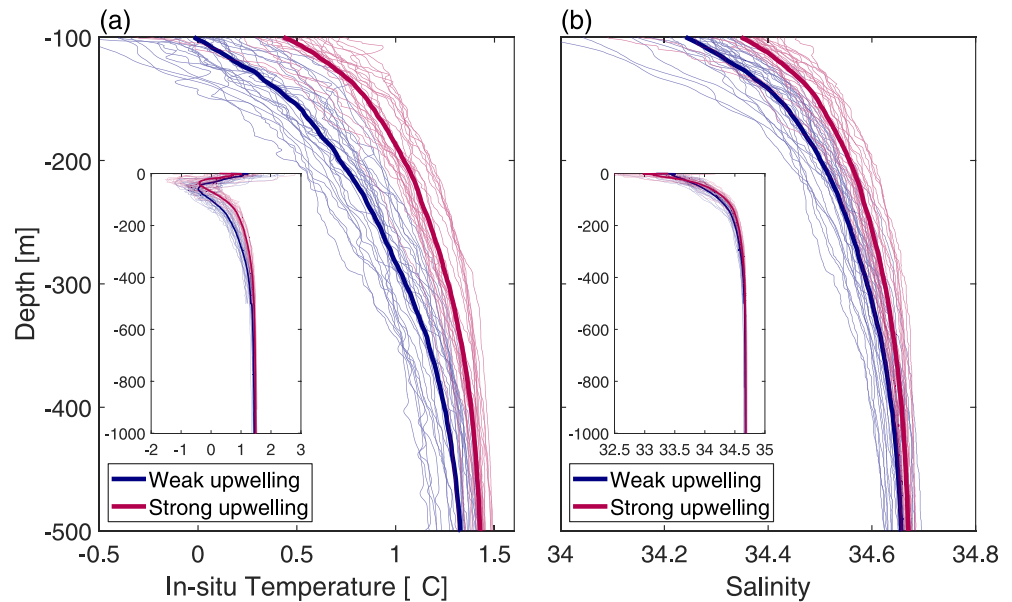
Figure 15. Summer profiles of in-situ temperature (a) and salinity (b) in Palmer Deep (the location is shown in Figure 1b) collected from 1993 to 2017. Color coded by the prevalent wind forcing conditions in Bransfield Strait during the previous winter. Red indicates strong upwelling-favorable conditions, blue are weak upwelling-to downwelling-favorable conditions. The thin lines indicate all the historical hydrographic data, and the thick lines show the averaged profiles. The insets show the hydrographic profiles with a 0–1,000 m depth range.

negative drive relatively more cold water into the cWAP, causing significant cooling. While the short model run does not permit fully exploring the interannual variability of these processes, they do suggest that variability in that timescale is considerable.

4. Discussion

4.1. Observational Evidence for Cooling Driven by Along-Shore Exchange

Analysis of the model output shows that the region in the cWAP adjacent to Bransfield Strait, where Palmer Station is located, receives significant cold water inflow in winter (Figure 5). While both the cWAP and Bransfield Strait are some of the most intensely sampled regions of Antarctica (e.g., the cWAP is home to the PAL-LTER), the shelf where the exchange is occurring and the SBF is formed falls in a gap between the most sustained observational efforts in the region. Moreover, the model shows the flooding of the cWAP occurring outside of the summer season, where most of the observational efforts in this region take place. As a result, observations to validate the model results are limited. We examine that limited data below.

We expect that winters, where weak upwelling-favorable winds are prevalent in Bransfield Strait, will result in colder deep temperatures in the northern cWAP the next summer. Figure 15 shows available vertical profiles collected in Palmer Deep (station 600.040 of PAL-LTER and the location is shown in Figure 1b) during summer. The profiles are color coded by the intensity of the upwelling-favorable winds in Bransfield Strait the previous winter calculated from the ERA5 winds. The profiles show that years with strong upwelling-favorable wind events have warmer and saltier water below 100 m. In years with weak upwelling-favorable conditions in Bransfield Strait, the averaged temperature decreases by about 0.25°C from 100 to 500 m, and the averaged salinity is 0.06 lower over the same depth range. This interannual variability from observed hydrographic properties supports the idea that wind forcing modulates the amount of cold water intruding into the northern cWAP, which is correlated to SAM, and that these intrusions have a measurable impact on the properties as far south as Palmer Station.

While our study shows that the island gaps and Boyd Strait are key pathways for exchange along the WAP, Gerlache Strait has long been recognized as a transition region between Bransfield Strait and the cWAP. Previous studies show the mCDW in the southern Gerlache and cold Bransfield Strait water dominating the northern part of the strait (e.g., da Cunha et al., 2018; Lundesgaard et al., 2020; Kerr et al., 2018; Parra et al., 2020). The model
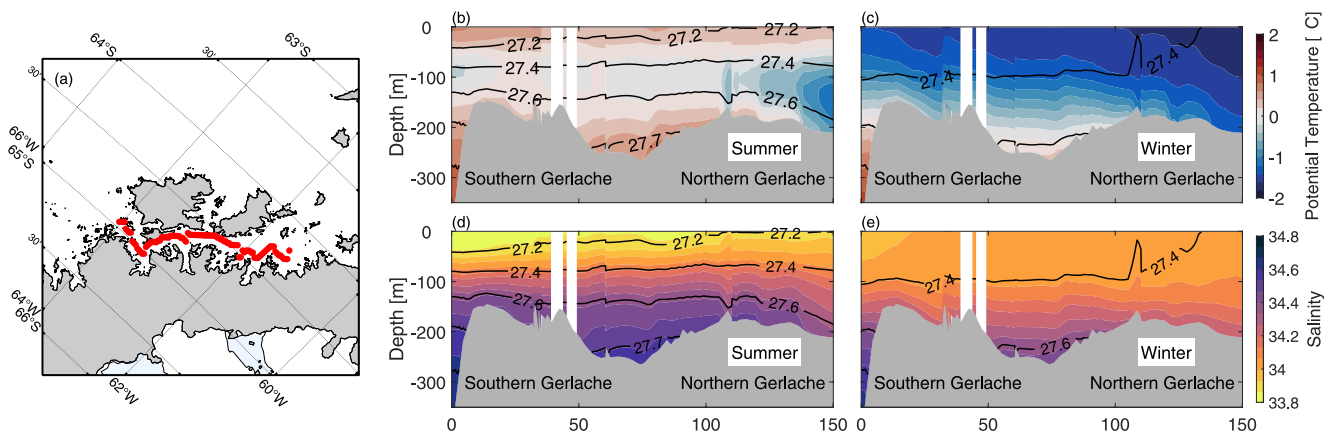
Figure 16. (a) Map shows the location of the along-shore section in Gerlache Strait, the section follows the deepest bathymetry of model output. Panels (b) and (c) show the mean water column distribution of potential temperature (°C) and salinity in summer, with isopycnals (kg/m³) overlaid. Panels (d) and (e) denote the water distribution averaged in winter.

output (Figure 16) is consistent with that general observed structure. However, we should note that the model bathymetry is fairly smooth in this region, and the horizontal resolution of the grid is unlikely to adequately simulate the details of the along-shore exchange here. Further improvements to the model configuration, including higher horizontal resolution and more accurate bathymetry, are necessary next steps to understand the role of the strait in the along-shore exchange.

Despite the potential shortcomings of a too-coarse, smooth-bathymetry model configuration in Gerlache Strait, the available data supports the mechanism of seasonal flooding of the cWAP from Bransfield Strait that we describe in Section 3.2. Mooring data collected in Andvord Bay (Lundesgaard et al., 2020) shows cooling of about 0.4°C at 300–500 m during winter. The authors interpreted this cooling as likely the result of deep convection, but our results suggest that the advection of Bransfield Strait water through Gerlache Strait could be an alternative cause of this observed cooling. In Figure 16, we show the average temperature at depth as a function of season and distance from the southern edge of Gerlache Strait. The model output clearly shows a strong difference (~1.5°C) between mCDW and cold Bransfield Strait water during the summer. A well documented structure during this season suggested a similar temperature difference of ~1.9°C at 350 db (Parra et al., 2020). While coverage is sparse the rest of the year, the data does show a much weaker temperature gradient and generally colder temperatures near the southern end of the strait, which is consistent with intruding water from Bransfield Strait. However, sustained, multi-seasonal observational records remain scarce, and efforts should be made to better understand the exchange processes in this region.

4.2. Implications for the Along-Shore Exchange in WAP

Our current understanding of the heat and salt budgets of the cWAP is based on a two-dimensional conceptual model where heat and salt influx from the Bellingshausen Sea is balanced by heat loss and freshening by air-sea interactions (including sea-ice formation and melting) and the melting of glaciers at the coast (Couto et al., 2017; Klinck, 1998; Moffat & Meredith, 2018). However, it is clear from our study that, at least in the northern cWAP, along-shore exchange is a key contributor to the heat budget. The input of cold water from Bransfield Strait affects the temperatures at depth, modulating the amount of heat available for vertical ventilation to the surface and for melting of marine terminating glaciers. Biochemical processes are also likely to be impacted by this along-shore exchange. The regional scale distribution and long-term evolution of chlorophyll along the WAP have a spatial pattern resembling the hydrographic structure discussed here (Montes-Hugo et al., 2009). Results from previous analysis using data collected at Rothera Station revealed that the extent of winter sea ice cover helps explain the reduction of the water column stratification the next summer (Venables et al., 2013). Those observations also showed that a more stable upper water column provides a favorable light environment for phytoplankton growth (Garibotti et al., 2003). In Palmer Deep, the analysis from underwater gliders suggests that the phytoplankton spring bloom is linked to water stability (Carvalho et al., 2016). How these processes will be impacted

by significant along-shore exchange, which brings waters to the northern cWAP that not only have different temperatures and salinity but also can modulate the vertical stratification of the water column, is an open question.

5. Summary

Here, we use 2 years of output from a high-resolution model of the WAP shelf to understand the magnitude and underlying dynamics of the along-shore exchange processes that result in the generation of strong along-shore property gradients on this shelf. Our results show strong seasonal variability of the along-shore water exchange process, which is characterized by the inflow of mCDW from the cWAP to Bransfield Strait during the summer, and a winter circulation dominated by flooding of the cWAP by cold waters entering Bransfield Strait from the Weddell Sea. The mCDW inflow to Bransfield Strait is carried in baroclinic, bottom intensified currents formed on the islands gaps separating the two exchanging regions. While some remnants remain in winter, the inflow is much stronger in summer. The structure of the Weddell-sourced water flowing along the WAP varies with seasons as well. The Weddell-sourced water transport from Bransfield Strait into the northern cWAP and Gerlache Strait has an increase of 7.0×10^5 m³/s from summer to winter. The analysis also shows this exchange can have significant interannual variability, which is modulated by winds in Bransfield Strait. When the along-shore wind stress is strongly upwelling-favorable, the resulting Ekman transport impedes the propagation of the coastal current toward the cWAP, advecting instead the relatively freshwater off the coast. When the winds become weakly upwelling-favorable or downwelling-favorable, the coastal current remains trapped against the coast, resulting in flooding of the cWAP by cold water from Bransfield Strait.

We also show that SAM plays a significant role in modulating these wind patterns, with positive values of the SAM index during winters (i.e., stronger westerlies) resulting in stronger upwelling-favorable winds in Bransfield Strait. Furthermore, we show that when cold water intrusions from Bransfield Strait do occur, they play a significant role in modulating the heat budget of the northern cWAP. While the data to validate our results is limited, particularly in the region north of Palmer Station and the southern boundary of Bransfield Strait where this exchange occurs, the available data does support the idea that there is significant interannual variability in the deep waters in this region (something that is not observed farther south in the cWAP). In the well-sampled (at least during summer) canyon off Palmer Deep, the data suggests colder deep waters are present in the summer when the winds are weakly upwelling-favorable in Bransfield Strait the previous winter, which is consistent with those years resulting in enhanced cold water intrusions to the northern cWAP. Overall, our results imply that while the cWAP has long been considered a warm Antarctic shelf (Thompson et al., 2018), Bransfield Strait acts as an extension of the Weddell Sea into the WAP, and the active exchange processes along the coast result in the northern cWAP being a transition region between the warm, southern cWAP and the cold Bransfield Strait.

While we have identified key, novel processes occurring along the WAP shelf, a number of questions remain unanswered that will be addressed in future work. Longer-term modeling runs should shed light on the extent of the interannual variability of the along-shore exchange processes, including the impact of variability in the inflow of water from the Weddell Sea, which was not significant in our 2-year output. Model improvements, including the horizontal resolution and bathymetry, the addition of tides, and the representation of runoff from the coast, are underway and will be incorporated in future work. Finally, efforts to collect data in the region where the along-shore front is found and where the exchange processes explored here are happening should be a priority if we are to understand how they impact the property budgets of this shelf.

Data Availability Statement

PAL-LTER data are available through the LTER website (https://pal.lternet.edu/data). APB data can be found from National Oceanographic Data Center (https://www.ncei.noaa.gov/access/world-ocean-database/bin/get-wodyearlydata.pl?Go=TimeSorted). Wind data can be accessed through https://cds.climate.copernicus.eu/cdsapp#!/dataset/reanalysis-era5-single-levels-monthly-means?tab=overview. The SAM index and Oceanic Niño index are available at https://legacy.bas.ac.uk/met/gjma/sam.html and https://origin.cpc.ncep.noaa.gov/products/analysis\text_monitoring/ensostuff/ONI_v5.php. The codes of the model are available from www.myroms.org.

References

Barlett, E. M. R., Tosonotto, G. V., Piola, A. R., Sierra, M. E., & Mata, M. M. (2018). On the temporal variability of intermediate and deep waters in the Western Basin of the Bransfield Strait. *Deep Sea Research Part II: Topical Studies in Oceanography*, *149*, 31–46. https://doi.org/10.1016/j.dsr2.2017.12.010

Boyer, T. P., Antonov, J. I., Baranova, O. K., Coleman, C., Garcia, H. E., Grodsky, A., & Zweng, M. M. (2013). *World ocean database 2013*. https://doi.org/10.7289/V5NZ85MT

Bromwich, D. H., Monaghan, A. J., Manning, K. W., & Powers, J. G. (2005). Real-time forecasting for the Antarctic: An evaluation of the Antarctic mesoscale Prediction system (AMPS). *Monthly Weather Review*, *133*(3), 579–603. https://doi.org/10.1175/MWR-2881.1

Budgell, W. (2005). Numerical simulation of ice-ocean variability in the Barents Sea region. *Ocean Dynamics*, *55*(3–4), 370–387. https://doi.org/10.1007/s10236-005-0008-3

Carton, J. A., & Giese, B. S. (2008). A reanalysis of ocean climate using Simple Ocean Data Assimilation (SODA). *Monthly Weather Review*, *136*(8), 2999–3017. https://doi.org/10.1175/2007MWR1978.1

Carvalho, F., Kohut, J., Oliver, M. J., Sherrell, R. M., & Schofield, O. (2016). Mixing and phytoplankton dynamics in a submarine canyon in the West Antarctic Peninsula. *Journal of Geophysical Research: Oceans*, *121*(7), 5069–5083. https://doi.org/10.1002/2016JC011650

Clem, K. R., Benjamin, R. L., Anthony, J. B., & James, R. M. (2019). Role of the South Pacific convergence zone in West Antarctic decadal climate variability. *Geophysical Research Letters*, *46*(12), 6900–6909. https://doi.org/10.1029/2019GL082108

Clem, K. R., & Fogt, R. L. (2013). Varying roles of ENSO and SAM on the Antarctic Peninsula climate in austral spring. *Journal of Geophysical Research: Atmospheres*, *118*(20), 11–481. https://doi.org/10.1002/jgrd.50860

Cook, A. J., Fox, A., Vaughan, D., & Ferrigno, J. (2005). Retreating glacier fronts on the Antarctic Peninsula over the past half-century. *Science*, *308*(5721), 541–544. https://doi.org/10.1126/science.1104235

Cook, A. J., Holland, P., Meredith, M., Murray, T., Luckman, A., & Vaughan, D. G. (2016). Ocean forcing of glacier retreat in the western Antarctic Peninsula. *Science*, *353*(6296), 283–286. https://doi.org/10.1126/science.aae0017

Couto, N., Martinson, D. G., Kohut, J., & Schofield, O. (2017). Distribution of upper Circumpolar deep water on the warming continental shelf of the west Antarctic peninsula. *Journal of Geophysical Research: Oceans*, *122*(7), 5306–5315. https://doi.org/10.1002/2017JC012840

da Cunha, L. C., Hamacher, C., Farias, C. d. O., Kerr, R., Mendes, C. R. B., & Mata, M. M. (2018). Contrasting end-summer distribution of organic carbon along the Gerlache Strait, northern Antarctic peninsula: Bio-physical interactions. *Deep Sea Research Part II: Topical Studies in Oceanography*, *149*, 206–217. https://doi.org/10.1016/j.dsr2.2018.03.003

Dee, D. P., Uppala, S. M., Simmons, A., Berrisford, P., Poli, P., Kobayashi, S., et al. (2011). The ERA-Interim reanalysis: Configuration and performance of the data assimilation system. *Quarterly Journal of the Royal Meteorological Society*, *137*(656), 553–597. https://doi.org/10.1002/qj.828

Dinniman, M. S., Klinck, J. M., & Hofmann, E. E. (2012). Sensitivity of Circumpolar Deep Water transport and ice shelf basal melt along the west Antarctic Peninsula to changes in the winds. *Journal of Climate*, *25*(14), 4799–4816. https://doi.org/10.1175/JCLI-D-11-00307.1

Dinniman, M. S., Klinck, J. M., & Smith, W. O., Jr. (2011). A model study of Circumpolar deep water on the west Antarctic peninsula and Ross sea continental shelves. *Deep Sea Research Part II: Topical Studies in Oceanography*, *58*(13–16), 1508–1523. https://doi.org/10.1016/j.dsr2.2010.11.013

Dotto, T. S., Kerr, R., Mata, M. M., & Garcia, C. A. (2016). Multidecadal freshening and lightening in the deep waters of the Bransfield Strait, Antarctica. *Journal of Geophysical Research: Oceans*, *121*(6), 3741–3756. https://doi.org/10.1002/2015JC011228

Dotto, T. S., Mata, M. M., Kerr, R., & Garcia, C. A. (2021). A novel hydrographic gridded data set for the Northern Antarctic Peninsula. *Earth System Science Data*, *13*(2), 671–696. https://doi.org/10.5194/essd-13-671-2021

Fogt, R. L., Bromwich, D. H., & Hines, K. M. (2011). Understanding the SAM influence on the south Pacific ENSO teleconnection. *Climate Dynamics*, *36*(7–8), 1555–1576. https://doi.org/10.1007/s00382-010-0905-0

Fretwell, P., Pritchard, H. D., Vaughan, D. G., Bamber, J. L., Barrand, N. E., Bell, R., et al. (2013). Bedmap2: Improved ice bed, surface and thickness datasets for Antarctica. *The Cryosphere*, *7*(1), 375–393. https://doi.org/10.5194/tc-7-375-2013

García, M. A., Castro, C. G., Ríos, A. F., Doval, M. D., Rosón, G., Gomis, D., & López, O. (2002). Water masses and distribution of physico-chemical properties in the western Bransfield Strait and Gerlache Strait during austral summer 1995/96. *Deep-Sea Research Part II Topical Studies in Oceanography*, *49*(4–5), 585–602. https://doi.org/10.1016/S0967-0645(01)00113-8

Garibotti, I. A., Vernet, M., Ferrario, M. E., Smith, R. C., Ross, R. M., & Quetin, L. B. (2003). Phytoplankton spatial distribution patterns along the western Antarctic peninsula (southern ocean). *Marine Ecology Progress Series*, *261*, 21–39. https://doi.org/10.3354/meps261021

Graham, J. A., Dinniman, M. S., & Klinck, J. M. (2016). Impact of model resolution for on-shelf heat transport along the West Antarctic Peninsula. *Journal of Geophysical Research: Oceans*, *121*(10), 7880–7897. https://doi.org/10.1002/2016JC011875

Haidvogel, D. B., Arango, H., Budgell, W. P., Cornuelle, B. D., Curchitser, E., Di Lorenzo, E., et al. (2008). Ocean forecasting in terrain-following coordinates: Formulation and skill assessment of the Regional Ocean modeling system. *Journal of Computational Physics*, *227*(7), 3595–3624. https://doi.org/10.1016/j.jcp.2007.06.016

Hersbach, H., Bell, B., Berrisford, P., Hirahara, S., Horányi, A., Muñoz-Sabater, J., et al. (2020). The ERA5 global reanalysis. *Quarterly Journal of the Royal Meteorological Society*, *146*(730), 1999–2049. https://doi.org/10.1002/qj.3803

Heywood, K. J., Naveira Garabato, A. C., Stevens, D. P., & Muench, R. D. (2004). On the fate of the Antarctic slope front and the origin of the Weddell front. *Journal of Geophysical Research: Oceans*, *109*(C6), C06021. https://doi.org/10.1029/2003JC002053

Hofmann, E. E., Klinck, J. M., Lascara, C. M., & Smith, D. A. (1996). Water mass distribution and circulation west of the Antarctic Peninsula and including Bransfield Strait. *Foundations for ecological research west of the Antarctic Peninsula*, *70*, 61–80. https://doi.org/10.1029/AR070p0061

Holland, D. M., & Jenkins, A. (1999). Modeling thermodynamic ice–ocean interactions at the base of an ice shelf. *Journal of Physical Oceanography*, *29*(8), 1787–1800. https://doi.org/10.1175/1520-0485(1999)029<1787:MTIOIA>2.0.CO;2

Jiang, M., Charette, M. A., Measures, C. I., Zhu, Y., & Zhou, M. (2013). Seasonal cycle of circulation in the Antarctic peninsula and the off-shelf transport of shelf waters into southern Drake Passage and Scotia sea. *Deep Sea Research Part II: Topical Studies in Oceanography*, *90*, 15–30. https://doi.org/10.1016/j.dsr2.2013.02.029

Kerr, R., Orselli, I. B., Lencina-Avila, J. M., Eidt, R. T., Mendes, C. R. B., da Cunha, L. C., & Tavano, V. M. (2018). Carbonate system properties in the Gerlache Strait, northern Antarctic peninsula (February 2015): I. Sea–Air CO2 fluxes. *Deep Sea Research Part II: Topical Studies in Oceanography*, *149*, 171–181. https://doi.org/10.1016/j.dsr.2017.02.008

Klinck, J. M. (1998). Heat and salt changes on the continental shelf west of the Antarctic Peninsula between January 1993 and January 1994. *Journal of Geophysical Research: Oceans*, *103*(C4), 7617–7636. https://doi.org/10.1029/98JC00369

Lentz, S. (2004). The response of buoyant coastal plumes to upwelling-favorable winds. *Journal of Physical Oceanography*, *34*(11), 2458–2469. https://doi.org/10.1175/JPO2647.1

Locarnini, R. A., Mishonov, A. V., Antonov, J. I., Boyer, T. P., Garcia, H. E., Baranova, O. K., et al. (2013). *World ocean atlas*, 2013, *1*. https://doi.org/10.7289/V55X26VD

López, O., García, M. A., Gomis, D., Rojas, P., Sospedra, J., & Sánchez-Arcilla, A. (1999). Hydrographic and hydrodynamic characteristics of the eastern basin of the Bransfield Strait (Antarctica). *Deep Sea Research Part I: Oceanographic Research Papers*, *46*(10), 1755–1778. https://doi.org/10.1016/S0967-0637(99)00017-5

Lundesgaard, Ø., Winsor, P., Truffer, M., Merrifield, M., Powell, B., et al. (2020). Hydrography and energetics of a cold subpolar fjord: Andvord Bay, western Antarctic Peninsula. *Progress in Oceanography*, *181*, 102224. https://doi.org/10.1016/j.pocean.2019.102224

Marshall, G. J. (2003). Trends in the southern Annular mode from observations and reanalyses. *Journal of Climate*, *16*(24), 4134–4143. 10.1175/1520-0442(2003)016<4134:TITSAM>2.0.CO;2

Martinson, D., & McKee, D. (2012). Transport of warm upper Circumpolar deep water onto the western Antarctic peninsula continental shelf. *Ocean Science*, *8*(4), 433–442. https://doi.org/10.5194/os-8-433-2012

Meredith, M. P., Stammerjohn, S. E., Venables, H. J., Ducklow, H. W., Martinson, D. G., Iannuzzi, R. A., & Barrand, N. E. (2017). Changing distributions of sea ice melt and meteoric water west of the Antarctic Peninsula. *Deep Sea Research Part II: Topical Studies in Oceanography*, *139*, 40–57. https://doi.org/10.1016/j.dsr2.2016.04.019

Moffat, C., Beardsley, R. C., Owens, B., & Van Lipzig, N. (2008). A first description of the Antarctic peninsula coastal current. *Deep Sea Research Part II: Topical Studies in Oceanography*, *55*(3–4), 277–293. https://doi.org/10.1016/j.dsr2.2007.10.003

Moffat, C., & Lentz, S. (2012). On the response of a buoyant plume to downwelling-favorable wind stress. *Journal of Physical Oceanography*, *42*(7), 1083–1098. https://doi.org/10.1175/JPO-D-11-015.1

Moffat, C., & Meredith, M. (2018). Shelf–ocean exchange and hydrography west of the Antarctic peninsula: A review. *Philosophical Transactions of the Royal Society A: Mathematical, Physical & Engineering Sciences*, *376*(2122), 20170164. https://doi.org/10.1098/rsta.2017.0164

Moffat, C., Owens, B., & Beardsley, R. (2009). On the characteristics of circumpolar deep water intrusions to the west Antarctic Peninsula continental shelf. *Journal of Geophysical Research: Oceans*, *114*(C5), C05017. https://doi.org/10.1029/2008JC004955

Montes-Hugo, M., Doney, S. C., Ducklow, H. W., Fraser, W., Martinson, D., Stammerjohn, S. E., & Schofield, O. (2009). Recent changes in phytoplankton communities associated with rapid regional climate change along the western Antarctic peninsula. *Science*, *323*(5920), 1470–1473. https://doi.org/10.1126/science.1164533

Niiler, P. P., Amos, A., & Hu, J.-H. (1991). Water masses and 200 m relative geostrophic circulation in the western Bransfield Strait region. Deep Sea Research Part A. *Oceanographic Research Papers*, *38*(8–9), 943–959. https://doi.org/10.1016/0198-0149(91)90091-S

Oliva, M., Navarro, F., Hrbáček, F., Hernandéz, A., Nỳvlt, D., Pereira, P., & Trigo, R. (2017). Recent regional climate cooling on the Antarctic Peninsula and associated impacts on the cryosphere. The *Science of the Total Environment*, *580*, 210–223. https://doi.org/10.1016/j.scitotenv.2016.12.030

Parra, R. R. T., Laurido, A. L. C., & Sánchez, J. D. I. (2020). Hydrographic conditions during two austral summer situations (2015 and 2017) in the Gerlache and Bismarck straits, northern Antarctic Peninsula. *Deep Sea Research Part I: Oceanographic Research Papers*, *161*, 103278. https://doi.org/10.1016/j.dsr.2020.103278

Powers, J. G., Manning, K. W., Bromwich, D. H., Cassano, J. J., & Cayette, A. M. (2012). A decade of Antarctic science support through AMPS. *Bulletin of the American Meteorological Society*, *93*(11), 1699–1712. https://doi.org/10.1175/BAMS-D-11-00186.1

Powers, J. G., Monaghan, A. J., Cayette, A. M., Bromwich, D. H., Kuo, Y.-H., & Manning, K. W. (2003). Real-time mesoscale modeling over Antarctica: The Antarctic mesoscale prediction system* The Antarctic mesoscale prediction system. *Bulletin of the American Meteorological Society*, *84*(11), 1533–1546. https://doi.org/10.1175/BAMS-84-11-1533

Renner, A. H., Thorpe, S. E., Heywood, K. J., Murphy, E. J., Watkins, J. L., & Meredith, M. P. (2012). Advective pathways near the tip of the Antarctic Peninsula: Trends, variability and ecosystem implications. *Deep Sea Research Part I: Oceanographic Research Papers*, *63*, 91–101. https://doi.org/10.1016/j.dsr.2012.01.009

Ross, R. M., Hofmann, E. E., & Quetin, L. B. (1996). *Foundations for Ecological Research West of the Antarctic Peninsula* (Vol. 70). American Geophysical Union Washington (DC). https://doi.org/10.1029/AR070

Sangrà, P., Gordo, C., Hernández-Arencibia, M., Marrero-Díaz, A., Rodríguez-Santana, A., Stegner, A., & Pichon, T. (2011). The Bransfield current system. *Deep-Sea Research Part I Oceanographic Research Papers*, *58*(4), 390–402. https://doi.org/10.1016/j.dsr.2011.01.011

Sangrà, P., Stegner, A., Hernández-Arencibia, M., Marrero-Díaz, Á., Salinas, C., et al. (2017). The Bransfield gravity current. *Deep Sea Research Part I: Oceanographic Research Papers*, *119*, 1–15. https://doi.org/10.1016/j.dsr.2016.11.003

Savidge, D. K., & Amft, J. A. (2009). Circulation on the west Antarctic peninsula derived from 6 years of shipboard ADCP transects. *Deep Sea Research Part I: Oceanographic Research Papers*, *56*(10), 1633–1655. https://doi.org/10.1016/j.dsr.2009.05.011

Schmidtko, S., Heywood, K. J., Thompson, A. F., & Aoki, S. (2014). Multidecadal warming of Antarctic waters. *Science*, *346*(6214), 1227–1231. DOI. https://doi.org/10.1126/science.1256117

Schmidtko, S., Johnson, G. C., & Lyman, J. M. (2013). Mimoc: A global monthly isopycnal upper-ocean climatology with mixed layers. *Journal of Geophysical Research: Oceans*, *118*(4), 1658–1672. https://doi.org/10.1002/jgrc.20122

Schubert, R., Thompson, A. F., Speer, K., Schulze Chretien, L., & Bebieva, Y. (2021). The Antarctic coastal current in the Bellingshausen Sea. *The Cryosphere Discussions*, 1–33. https://doi.org/10.5194/tc-15-4179-2021

Schultz, C., Doney, S. C., Zhang, W. G., Regan, H., Holland, P., Meredith, M., & Stammerjohn, S. (2020). Modeling of the influence of sea ice cycle and Langmuir circulation on the upper ocean mixed layer depth and freshwater distribution at the West Antarctic Peninsula. *Journal of Geophysical Research: Oceans*, *125*(8), e2020JC016109. https://doi.org/10.1029/2020JC016109

Shchepetkin, A. F., & McWilliams, J. C. (2003). A method for computing horizontal pressure-gradient force in an oceanic model with a nonaligned vertical coordinate. *Journal of Geophysical Research: Oceans*, *108*(C3), 3090. https://doi.org/10.1029/2001JC001047

Shchepetkin, A. F., & McWilliams, J. C. (2005). The regional oceanic modeling system (ROMS): A split-explicit, free-surface, topography-following-coordinate oceanic model. *Ocean Modelling*, *9*(4), 347–404. https://doi.org/10.1016/j.ocemod.2004.08.002

Shchepetkin, A. F., & McWilliams, J. C. (2009). Correction and commentary for "Ocean forecasting in terrain-following coordinates: Formulation and skill assessment of the regional ocean modeling system" by Haidvogel et al. *Journal of Computational Physics*, *228*(24), 8985–9000. https://doi.org/10.1016/j.jcp.2009.09.002

Smith, D. A., Hofmann, E. E., Klinck, J. M., & Lascara, C. M. (1999). Hydrography and circulation of the west Antarctic Peninsula continental shelf. *Deep Sea Research Part I: Oceanographic Research Papers*, *46*(6), 925–949. https://doi.org/10.1016/S0967-0637(98)00103-4

Smith, D. A., & Klinck, J. M. (2002). Water properties on the West Antarctic peninsula continental shelf: A model study of effects of surface fluxes and sea ice. *Deep Sea Research Part II: Topical Studies in Oceanography*, *49*(21), 4863–4886. https://doi.org/10.1016/S0967-0645(02)00163-7

Smith, R. C., Fraser, W. R., Stammerjohn, S. E., & Vernet, M. (2003). Palmer long-term ecological research on the Antarctic marine ecosystem. *Antarctic Research Series*, *79*, 131–144. https://doi.org/10.1029/AR079P0131

Stammerjohn, S. E., Martinson, D. G., Smith, R. C., & Iannuzzi, R. A. (2008). Sea ice in the western Antarctic Peninsula region: Spatio-temporal variability from ecological and climate change perspectives. *Deep Sea Research Part II: Topical Studies in Oceanography*, *55*(18–19), 2041–2058. https://doi.org/10.1016/j.dsr2.2008.04.026

Sutherland, D. A., & Pickart, R. S. (2008). The East Greenland coastal current: Structure, variability, and forcing. *Progress in Oceanography*, *78*(1), 58–77. https://doi.org/10.1016/j.pocean.2007.09.006

Thompson, A. F., Heywood, K. J., Thorpe, S. E., Renner, A. H., & Trasviña, A. (2009). Surface circulation at the tip of the Antarctic Peninsula from drifters. *Journal of Physical Oceanography*, *39*(1), 3–26. https://doi.org/10.1175/2008JPO3995.1

Thompson, A. F., Stewart, A. L., Spence, P., & Heywood, K. J. (2018). The Antarctic slope current in a changing climate. *Reviews of Geophysics*, *56*(4), 741–770. https://doi.org/10.1029/2018RG000624

Tokarczyk, R. (1987). Classification of water masses in the Bransfield Strait and southern part of the Drake Passage using a method of statistical multidimensional analysis. *International Journal of Climatology*, *25*(3), 333–366.

Turner, J., Colwell, S. R., Marshall, G. J., Lachlan-Cope, T. A., Carleton, A. M., Jones, P. D., & Iagovkina, S. (2005). Antarctic climate change during the last 50 years. *International Journal of Climatology*, *25*(3), 279–294. https://doi.org/10.1002/joc.1130

Turner, J., Lu, H., White, I., King, J. C., Phillips, T., Hosking, J. S., & Deb, P. (2016). Absence of 21st century warming on Antarctic Peninsula consistent with natural variability. *Nature*, *535*(7612), 411–415. https://doi.org/10.1038/nature18645

Turner, J., Phillips, T., Hosking, J. S., Marshall, G. J., & Orr, A. (2013). The amundsen sea low. *International Journal of Climatology*, *33*(7), 1818–1829. https://doi.org/10.1002/joc.3558

Van Lipzig, N., King, J., Lachlan-Cope, T., & Van den Broeke, M. (2004). Precipitation, sublimation, and snow drift in the Antarctic Peninsula region from a regional atmospheric model. *Journal of Geophysical Research: Atmospheres*, *109*(D24), D24106. https://doi.org/10.1029/2004JD004701

van Wessem, J. M., Reijmer, C. H., van de Berg, W. J., Van den Broeke, M., Cook, A. J., van Ulft, L. H., & van Meijgaard, E. (2015). Temperature and wind climate of the Antarctic Peninsula as simulated by a high-resolution regional atmospheric climate model. *Journal of Climate*, *28*(18), 7306–7326. https://doi.org/10.1175/JCLI-D-15-0060.1

Vaughan, D. G., Marshall, G. J., Connolley, W. M., Parkinson, C., Mulvaney, R., Hodgson, D. A., & Turner, J. (2003). Recent rapid regional climate warming on the Antarctic Peninsula. *Climatic Change*, *60*(3), 243–274. https://doi.org/10.1023/A:1026021217991

Venables, H. J., Clarke, A., & Meredith, M. P. (2013). Wintertime controls on summer stratification and productivity at the western Antarctic Peninsula. *Limnology & Oceanography*, *58*(3), 1035–1047. https://doi.org/10.4319/lo.2013.58.3.1035

von Gyldenfeldt, A.-B., Fahrbach, E., García, M. A., & Schröder, M. (2002). Flow variability at the tip of the Antarctic peninsula. *Deep Sea Research Part II: Topical Studies in Oceanography*, *49*(21), 4743–4766. https://doi.org/10.1016/S0967-0645(02)00157-1

Yuan, X. (2004). ENSO-related impacts on Antarctic sea ice: A synthesis of phenomenon and mechanisms. *Antarctic Science*, *16*(4), 415–425. https://doi.org/10.1017/S0954102004002238

Zhou, M., Niiler, P. P., & Hu, J. H. (2002). Surface currents in the Bransfield and Gerlache straits, Antarctica. *Deep-Sea Research Part I Oceanographic Research Papers*, *49*(2), 267–280. https://doi.org/10.1016/S0967-0637(01)00062-0

Zhou, M., Niiler, P. P., Zhu, Y., & Dorland, R. D. (2006). The western boundary current in the Bransfield Strait, Antarctica. *Deep Sea Research Part I: Oceanographic Research Papers*, *53*(7), 1244–1252. https://doi.org/10.1016/j.dsr.2006.04.003

Zweng, M. M., Reagan, J. R., Antonov, J. I., Locarnini, R. A., Mishonov, A. V., Boyer, T. P., & Biddle, M. M. (2013). *World Ocean Atlas 2013* (Vol. 2), salinity. https://doi.org/10.7289/V5251G4D